

Response to Reviewer Comments

Title: Elucidating the pollution characteristics of nitrate, sulfate and ammonium in PM_{2.5} in Chengdu, southwest China, based on three-year measurements

Minor revisions:

This concerns text on lines 262-275:

The sentence starting on line 265 "The phenomenon...". This is a confusing statement. You mean that this result occurs because not all chemical species are well constrained? This needs a bit more elaboration, so the reader can understand this.

This other point is: It seems that you refer to a study reporting lower organic fraction at high PM_{2.5}, but in that case, one of the reviewer believes that the inorganic fraction is increased. It thus cannot explain the decrease of the inorganic fraction here. Could you please explain the reasons for the reduced inorganic fraction and what other chemical compounds (e.g., dust particle) may contribute to that.

Response:

We appreciate your comments and apologize for our unprofessional description. We re-examined this description and found that the description was indeed inappropriate and prone to misunderstanding. With the accumulation of PM_{2.5} concentration, NSA, OC, EC and metal element concentrations have an increasing trend, but their ratio with PM_{2.5} gradually decreases, indicating that other components have a higher contribution. Studies have shown that the contribution of unknown components in PM_{2.5} has a higher proportion, such as in Xi'an (29.5-38.2%) and Chengdu (16.5-33.8%), and under higher PM_{2.5} concentration conditions, the proportion increases (Huang et al., 2014; Li et al., 2017). Also, under the implementation of the Air Pollution Prevention and Control Action Plan (2013-2017), the PM_{2.5} concentration was significantly reduced in 2017 compared with 2013, and the contribution of unknown components of its chemical composition to PM_{2.5} was reduced, such as eastern China (from 22% down to 20%), Beijing-Tianjin-Hebei (from 24% down to 23%) and the Yangtze River Delta (from 24% down to 22%) also show that the contribution of unknown components at higher PM_{2.5} concentrations will increase (Geng et al., 2019). Therefore, our analysis results, on the one hand, can be attributed to those chemical compositions such as ions and mineral dust which are not included in the statistics (Huang et al., 2014; Zhang et al., 2015), and

on the other hand, can be attributed to the contribution of unknown components.

So we revised the description in the manuscript, Now, it reads as follows:

The chemical compositions of PM_{2.5} from 2015 to 2017 varies with concentration, as shown in Fig. 2. With the accumulation of PM_{2.5} in the atmosphere, the concentration of NSA also increased significantly, but the proportion of NSA in PM_{2.5} decreased (Fig. 2a and b). The variation trend of OC, EC and metal elements with increasing PM_{2.5} concentration is similar to that of NSA (Fig. 2c and d), and this variation trend of OC and EC is consistent with the results of long-term observation research carried out in Beijing (Ji et al., 2019). With the accumulation of PM_{2.5} concentration, NSA, OC, EC and metal element concentrations have an increasing trend, but their ratio with PM_{2.5} gradually decreases, indicating that other compositions have a higher contribution. This result, on the one hand, maybe since some chemical compositions such as ions and dust have not included in the statistics, on the other hand, the unknown component may also have a high contribution characteristic to PM_{2.5} (Zhang et al., 2015;Huang et al., 2014). For the contribution characteristics of unknown components of PM_{2.5}, studies in some regions of China show that the contribution of higher PM_{2.5} concentration is higher than that of lower PM_{2.5} concentration (Huang et al., 2014;Li et al., 2017;Geng et al., 2019).

References:

- Geng, G., Xiao, Q., Zheng, Y., Tong, D., Zhang, Y., Zhang, X., Zhang, Q., He, K., and Liu, Y.: Impact of China's Air Pollution Prevention and Control Action Plan on PM_{2.5} chemical composition over eastern China, *Science China Earth Sciences*, 62, 1872-1884, 10.1007/s11430-018-9353-x, 2019.
- Huang, R. J., Zhang, Y., Bozzetti, C., Ho, K. F., Cao, J. J., Han, Y., Daellenbach, K. R., Slowik, J. G., Platt, S. M., Canonaco, F., Zotter, P., Wolf, R., Pieber, S. M., Bruns, E. A., Crippa, M., Ciarelli, G., Piazzalunga, A., Schwikowski, M., Abbaszade, G., Schnelle-Kreis, J., Zimmermann, R., An, Z., Szidat, S., Baltensperger, U., El Haddad, I., and Prevot, A. S.: High secondary aerosol contribution to particulate pollution during haze events in China, *Nature*, 514, 218-222, 10.1038/nature13774, 2014.
- Ji, D., Gao, W., Maenhaut, W., He, J., Wang, Z., Li, J., Du, W., Wang, L., Sun, Y., Xin, J., Hu, B., and Wang, Y.: Impact of air pollution control measures and regional transport on carbonaceous aerosols in fine particulate matter in urban Beijing, China: insights gained from long-term measurement, *Atmospheric Chemistry and Physics*, 19, 8569-8590, 10.5194/acp-19-8569-2019, 2019.

- Li, L., Tan, Q., Zhang, Y., Feng, M., Qu, Y., An, J., and Liu, X.: Characteristics and source apportionment of PM_{2.5} during persistent extreme haze events in Chengdu, southwest China, *Environmental Pollution*, 230, 718-729, 10.1016/j.envpol.2017.07.029, 2017.
- Zhang, R., Wang, G., Guo, S., Zamora, M. L., Ying, Q., Lin, Y., Wang, W., Hu, M., and Wang, Y.: Formation of urban fine particulate matter, *Chemical Reviews*, 115, 3803-3855, 10.1021/acs.chemrev.5b00067, 2015.

1 **Elucidating the pollution characteristics of nitrate, sulfate and ammonium in**
2 **PM_{2.5} in Chengdu, southwest China, based on three-year measurements**

3 Liuwei Kong¹, Miao Feng², Yafei Liu¹, Yingying Zhang¹, Chen Zhang¹, Chenlu Li¹, Yu
4 Qu³, Junling An³, Xingang Liu^{1,*}, Qinwen Tan^{2,*}, Nianliang Cheng⁴, Yijun Deng⁵,
5 Ruixiao Zhai⁵, Zheng Wang⁵

6 ¹State Key Laboratory of Water Environment Simulation, School of Environment,
7 Beijing Normal University, Beijing 100875, China

8 ²Chengdu Academy of Environmental Sciences, Chengdu 610072, China

9 ³State Key Laboratory of Atmospheric Boundary Layer Physics and Atmospheric
10 Chemistry, Institute of Atmospheric Physics, Chinese Academy of Sciences, Beijing
11 100029, China

12 ⁴Beijing Municipal Environmental Monitoring Center, Beijing 100048, China

13 ⁵Yuncheng Municipal Ecological Environment Bureau, Yuncheng, 044000, China

14 * Corresponding author.

15 E-mail addresses: liuxingang@bnu.edu.cn (Xingang Liu) and 11923345@qq.com
16 (Qinwen Tan)

17 **Abstract**

18 Nitrate, sulfate and ammonium (NSA) are the main secondary inorganic aerosols of
19 PM_{2.5} and play an important role in air pollution. In this study, a three-year
20 observational experiment was conducted from January 1, 2015, to December 31, 2017,
21 in Chengdu, southwest China. NSA pollution characteristics, chemical conversion
22 generation, emission reduction control sensitivity and pollutant regional transport
23 characteristics were analysed. NSA are the most important chemical compositions of
24 particles with aerodynamic equivalent diameter $\leq 2.5 \mu\text{m}$ in ambient air (PM_{2.5}), and
25 the contribution of nitrate to the accumulation of PM_{2.5} concentration is greater than
26 that of sulfate and ammonium. NSA also have obvious characteristics of annual,
27 monthly, seasonal, diurnal and weekly variations. Through observation data and model
28 simulation, it was also found that the existence of an aerosol aqueous environment plays

29 an important role in the formation and existence of NSA. Sensitivity analysis between
30 NSAs found that controlling NO_3^- and SO_4^{2-} play an important role in reducing the
31 contribution of NSA to $\text{PM}_{2.5}$, which also implies that the current control of NO_x and
32 SO_2 is important for improving air pollution. Combined with meteorological conditions
33 and potential source contribution function (PSCF) analysis, local emissions and
34 regional emissions of pollutants are found to have important impacts on Chengdu's
35 atmospheric environment. This research result not only provides an assessment of the
36 current atmospheric emission reduction effect but also provides an important reference
37 for atmospheric pollution control.

38 **Keywords:** Secondary inorganic aerosols; Three-year measurements; Pollution
39 characteristics; Chemical conversions; Regional transport; Chengdu

40 **1 Introduction**

41 In recent years, with the rapid development of China's domestic economy and
42 acceleration of urbanization, energy consumption and pollutant emissions have also
43 increased, which increases the burden on the atmospheric environment, and severe air
44 pollution has become a focus of social concern (Liu et al., 2013a; An et al., 2019; Fu et
45 al., 2014; Zhao et al., 2017). When air pollution forms, mass concentrations of particles
46 with aerodynamic equivalent diameter $\leq 2.5 \mu\text{m}$ in ambient air ($\text{PM}_{2.5}$, also known as
47 fine particles) can reach a higher pollution level, which not only reduces atmospheric
48 visibility but also carries a large number of toxic species into the human lungs,
49 increasing the risks of cardiovascular and cerebrovascular diseases (Chang et al.,
50 2018; Tie et al., 2009; Kong et al., 2019; Zhao et al., 2018; Yang et al., 2015a). Nitrate,
51 sulfate, ammonium, organic matter and elemental carbon are the main compositions of
52 $\text{PM}_{2.5}$, among which nitrate, sulfate and ammonium (NSA) are the main secondary
53 inorganic aerosols in $\text{PM}_{2.5}$ (Ji et al., 2019; Zheng et al., 2016). NSA mainly originates
54 from the secondary aerosols produced by complex chemical reactions of NO_x , SO_2 and
55 NH_3 from coal combustion, vehicle exhaust emissions and agricultural sources (Liu et
56 al., 2013b; Wang et al., 2016; Tian et al., 2017).

57 Because China's current main energy resource is still fossil fuels, which are widely used
58 in industry, for vehicles and residentially, the emission reduction space of NSA is still
59 restricted by a large number of gaseous precursors of NSA (Zhao et al., 2018; Tong et
60 al., 2019). In addition, the chemical conversion of NO₂, SO₂ and NH₃ to form NSA is
61 still very complex, and both homogeneous and heterogeneous reactions involve the
62 chemical conversion of secondary inorganic aerosols, such as photochemical reactions,
63 aqueous phase oxidation environments of aerosols and catalysis of mineral dust (Cheng
64 et al., 2016; Sun et al., 2014; Wang et al., 2016; Ohta and Okita, 1990; He et al., 2014).
65 The formation of sulfate can increase the acidity of aerosols (Sun et al., 2014). In
66 contrast, the presence of NH₃ can play a role in neutralization and maintain the acid-
67 base balance of aerosols (Wang et al., 2016). If improper control measures are taken in
68 pollution reduction control, such as further ammonia emission reduction, the
69 acidification of aerosols and environmental problems of acid rain may be aggravated
70 (Liu et al., 2019c). In addition to the air pollution caused by the local emission of
71 pollutants, the regional transportation of pollutants from its surrounding cities also has
72 an important impact on the urban air quality. Determination of regional transport
73 sources of pollutants, taking regional joint prevention and control measures, and jointly
74 reducing the emissions of pollutants will enable better air control effects, particularly
75 in the Beijing-Tianjin-Hebei region of northern China (Chen et al., 2019a).
76 Higher concentrations of NSA in PM_{2.5} were also found in regions with more serious
77 air pollution in China, such as Beijing-Tianjin-Hebei, the Yangtze River Delta, the Pearl
78 River Delta, the Fenwei Plain, and the Chengdu-Chongqing region (An et al., 2019; Li
79 et al., 2017; Liu et al., 2019d). In response to this situation, the Chinese government
80 issued an Air Pollution Prevention and Control Action Plan (2013-2017) in 2013 to
81 reduce pollutant emissions and improve air quality (the State Council, 2013, last access:
82 June 17, 2020). A large number of treatment measures have been taken regarding coal
83 combustion, motor vehicle emissions and outdated industrial capacities, and by 2017,
84 China's ambient air quality control measures had achieved good results (Liu et al.,

85 2019a;Chen et al., 2019b;Cheng et al., 2019;Li et al., 2019a). In Beijing, PM_{2.5}, NO₂
86 and SO₂ decreased by 35.2%, 17.9% and 69.8%, respectively, in 2017 compared with
87 2013 (Beijing Municipal Ecology and Environment Bureau, 2018, last access: June 17,
88 2020). In Chengdu, PM_{2.5}, NO₂ and SO₂ decreased by 42.3%, 15.9% and 64.5%,
89 respectively, in 2017 compared with 2013 (Chengdu Municipal Ecology and
90 Environment Bureau, 2018, last access: June 17, 2020). To continue to promote air
91 quality improvement, the Chinese government launched the "Three-Year Action Plan
92 for Winning the Blue Sky Defense Battle" in 2018, which puts forward stricter
93 requirements on how to further promote the implementation of emission reduction
94 plans (the State Council, 2018, last access: June 17, 2020). Through long-term
95 observations, a comprehensive analysis of PM_{2.5} chemical compositions and source
96 characteristics is carried out to verify the current implementation effects of emission
97 reduction, and in-depth analyses of pollution reduction control characteristics are of
98 great significance for the next step in air pollution control. However, these analyses
99 may be affected by the experimental equipment, observation stations and other
100 conditions, and the time span of these atmospheric observations usually includes
101 several pollution processes or lasts for weeks or months. Thus, it is difficult to analyse
102 the long-term variations in characteristics of air pollution through comprehensive
103 observation. In particular, there are few high-time-resolution (1 hour) observation
104 experiments carried out with online automatic observation systems (Sun et al., 2013;Tie
105 et al., 2017;Guo et al., 2014). Especially in the Sichuan Basin of southwest China, there
106 are few long-term observational experiments on NSA, which are the main chemical
107 compositions of PM_{2.5}.

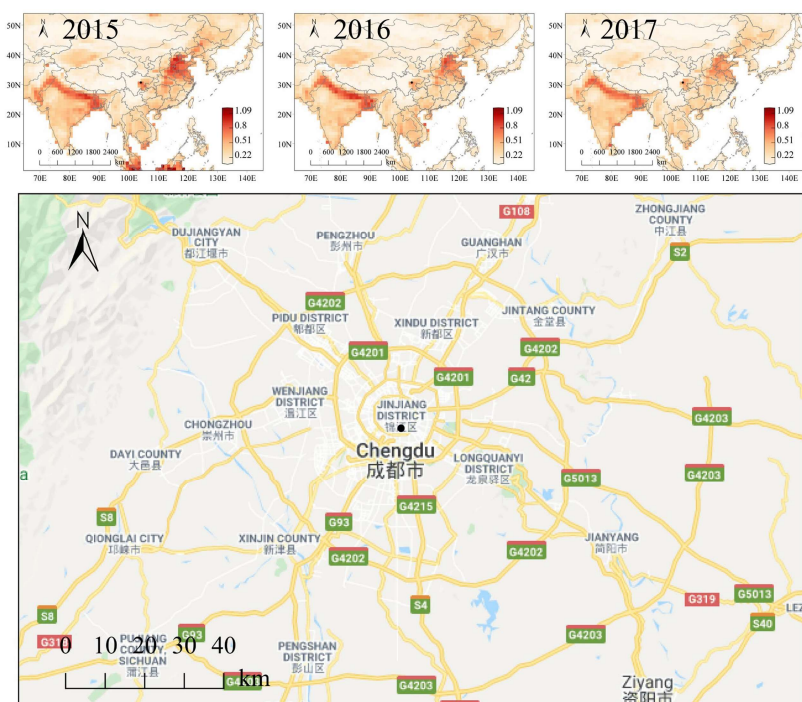
108 The Sichuan Basin is among the most important areas of air pollution in China (Qiao
109 et al., 2019;Gui et al., 2019;Zhong et al., 2019). Although there are many studies in this
110 area, there are few long-term studies of the hourly concentration data resolution of
111 PM_{2.5} chemical compositions. In this study, through three years of observations (from
112 January 1, 2015, to December 31, 2017), we analysed the pollution characteristics of

113 NSA, as well as their formation mechanism and pollution control sensitivity. Finally,
114 combined with local emissions and regional transport characteristics, we analysed the
115 air pollution transport characteristics of Chengdu air pollution.

116 **2 Experiment and methods**

117 **2.1 Observation site**

118 Comprehensive observations were carried out at the Chengdu comprehensive
119 observation station of atmospheric combined pollution (30.63°N, 104.08°E). The
120 observation equipment was placed on the top of a building, approximately 25 m from
121 the ground, and there was no obvious pollution source within approximately 200 m.
122 The site is located in south section 1 of Yihuan Road, Wuhou District, Chengdu (Fig.
123 1), and traffic emission sources may be the main pollution emission source around the
124 observation station. This is a typical residential, traffic and commercial mixed area that
125 represents the characteristics of the urban atmospheric environment. Chengdu is also a
126 megacity in the Sichuan Basin of southwest China, as well as an important part of the
127 Chengdu-Chongqing region, which is among the regions with serious air pollution in
128 China, and as shown in Fig. 1, the Sichuan Basin also has high aerosol optical depth
129 (AOD).



130

131 Fig. 1. Observation site in Chengdu. The image on the top shows the aerosol optical
 132 depth (AOD, 550 nm) from 2015 to 2017 (National Aeronautics and Space
 133 Administration, 2019, last access: June 17, 2020). The black dot in the image on the
 134 bottom shows the location of the observation site in Chengdu (background map from
 135 Google Maps, last access: June 17, 2020).

136 2.2 Instruments

137 During the research period, online experimental monitoring instruments were used to
 138 obtain the observation data with an hourly resolution (1 hour). The equipment list is
 139 shown in Table 1. Data quality control and assurance are an important part of the
 140 atmospheric comprehensive observation experiment, and this result is described in
 141 detail in the supplementary materials (Fig. S1-4).

142 Table 1. The experimental instruments used in this study

Instruments	Parameters	Manufacturer/Country
URG-9000	NO ₃ ⁻ /SO ₄ ²⁻ /NH ₄ ⁺ /Na ⁺ /Mg ²⁺ /Ca ²⁺ /Cl ⁻ /K ⁺	Thermo Fisher Scientific/USA
SHARP 5030	PM _{2.5}	Thermo Fisher Scientific/USA
RT-4	OC/EC	Sunset Laboratory/USA
Xact-625	Metal elements	Cooper Environmental Services /USA
17i/450i/48i/49i	NO _x /NO ₂ /NO/NH ₃ /SO ₂ /CO/O ₃	Thermo Fisher Scientific/USA
WXT520	Meteorological parameters	VAISALA/Germany

带格式的: 字体: 五号

OC: organic carbon; EC: element carbon

143 2.3 Chemical conversions and model methods

144 To clarify the conversion of gaseous pollutants to secondary aerosols, the nitrogen
 145 oxidation ratio (NOR) and sulfur oxidation ratio (SOR) were used to reflect the
 146 conversions of NO₂ and SO₂ to NO₃⁻ and SO₄²⁻, respectively (Sun et al., 2014; Yang et
 147 al., 2015a). These ratios can be calculated using Eq. (1) and Eq. (2):

$$148 \text{ NOR} = \frac{n\text{NO}_3^-}{n\text{NO}_3^- + n\text{NO}_2} \quad (1)$$

$$149 \text{ SOR} = \frac{n\text{SO}_4^{2-}}{n\text{SO}_4^{2-} + n\text{SO}_2} \quad (2)$$

150 where n is the molar concentration.

151 The ISORROPIA-II thermodynamic model was used to analyse the variation in
 152 interaction characteristics among aerosol chemical compositions (Fountoukis and
 153 Nenes, 2007; Guo et al., 2017a; Ding et al., 2019). Temperature (T), relative humidity
 154 (RH) and the concentrations of Na⁺, SO₄²⁻, NH₃, NO₃⁻, Cl⁻, Ca²⁺, K⁺ and Mg²⁺ were
 155 input into the ISORROPIA-II thermodynamic equilibrium model. In this study, we used
 156 the “forward problems” mode to run the model, assuming that the aerosols were in a
 157 “metastable” state (salts do not precipitate under supersaturated conditions). At the time
 158 of data input, NH₃ data were the sum of NH₃ and NH₄⁺. Previous studies had shown
 159 that the model has better performance when the RH is greater than 30%, and some
 160 studies also believe that the model performance is greater than 40%, so this study
 161 maintains the RH at higher than 40% when data are input (Ding et al., 2019; Guo et al.,
 162 2016). The simulated data and observed data were compared and analysed, and the

163 observation data of NH₃ were consistent with the input data of the model. The linear
164 regression fitting slope of NH₃ was 0.96 (R²=0.98), which showed that the run result of
165 the model had good reliability and performance (Ding et al., 2019). Simultaneously, the
166 aerosol water content (AWC) was calculated, and the sensitivity of the interaction
167 between aerosol chemical compositions (NSA) and the pH of aerosols was analysed
168 (Ding et al., 2019; Fountoukis et al., 2009). The pH was calculated using Eq. (3):

$$169 \text{ pH} = -\log_{10} H_{\text{aq}}^+ \cong -\log_{10} \frac{1000 H_{\text{air}}^+}{\text{AWC}} \quad (3)$$

170 where H_{aq}⁺ (mol/L) is the concentration of hydronium ions in liquid water of
171 atmospheric particulate matter, which can be calculated by the H_{air}⁺ and AWC (μg/m³)
172 outputs from the ISORROPIA-II thermodynamic equilibrium model (Ding et al.,
173 2019; Guo et al., 2017a).

174 **2.4 CPF and PSCF methods**

175 We used the conditional probability function (CPF) to analyse the characteristics of
176 pollutants under the influence of wind direction (WD) and wind speed (WS). The
177 analysis results using CPF were obtained using the R programming language, named
178 openair. This function can be defined as CPF = m_{θ,j}/n_{θ,j}, where m_{θ,j} is the number of
179 samples in the WD interval θ and WS interval j with mixing ratios greater than some
180 ‘high’ pollution concentration, and n_{θ,j} is the total number of samples in the same WD-
181 WS interval (Uria-Tellaetxe and Carslaw, 2014). Usually, a higher given ‘high’
182 pollution concentration (percentile) is chosen, such as the 90th percentile, which will
183 mask the lower percentile pollution concentration source contributions. In this work, to
184 obtain a more complete contribution of pollution sources, a range of percentile values,
185 0-25, 25-50, 50-75 and 75-100 were selected for the CPF calculation.

186 The potential source contribution function (PSCF) is based on an analysis of pollution
187 sources given the air mass backward trajectory and can be used to judge the long-
188 distance regional transport of pollutants (Ji et al., 2019). In this study, MeteoInfoMap
189 and TrajStat (Wang et al., 2009) were used, and the model simulation data input model
190 was provided by the National Oceanic and Atmospheric Administration (National

191 Oceanic and Atmospheric Administration, 2019, last access: June 17, 2020); these data
 192 were calculated to the 24-hour backward trajectories at the observation site at a height
 193 of 500 m every 1 hour from January 1, 2015, to December 31, 2017 (UTC+8). The
 194 calculated domain for PSCF was a range of 20-50° N, 75-115° E, and a grid cell with
 195 a resolution of 0.5°×0.5° was divided. The PSCF could be defined using Eq. (4):

$$196 \text{ PSCF}_{ij} = \frac{M_{ij}}{N_{ij}} W_{ij} \quad (4)$$

$$197 W_{ij} = \begin{cases} 1.0 & (N_{ij} \geq 3N_{ave}) \\ 0.7 & (3N_{ave} > N_{ij} \geq 1.5N_{ave}) \\ 0.4 & (1.5N_{ave} > N_{ij} \geq N_{ave}) \\ 0.2 & (N_{ave} > N_{ij}) \end{cases} \quad (5)$$

198 where PSCF_{ij} is the value for the ijth grid cell and M_{ij} is the total number of endpoints
 199 in the ijth grid cell, with pollution concentrations at the observation site (30.63°N,
 200 104.08°E) that are greater than a given threshold value (the 75th percentile was selected
 201 for gaseous pollutants). N_{ij} is the number of backward trajectory endpoints in the ijth
 202 grid cell (0.5°×0.5°) during the simulation period. Therefore, the PSCF reflects the two-
 203 dimensional planar position distribution characteristics of potential sources, not the
 204 three-dimensional characteristics that reflect the transmission of pollution. To reduce
 205 the uncertainty in N_{ij}, the empirical weight function W_{ij} was introduced in Eq. (5),
 206 where N_{ave} is the average of N_{ij} during the simulation period (Ji et al., 2019; Zhang et
 207 al., 2017; Wang et al., 2009).

208 **3 Results and discussion**

209 **3.1 Pollution characteristics of the interannual and entire observation periods**

210 The annual average mass concentration of NSA and its proportion in PM_{2.5} are shown
 211 in Table 2. The annual averages of PM_{2.5} were 67.78, 71.88 and 59.68 μg/m³,
 212 corresponding to 2015, 2016 and 2017, respectively. However, the pollution of PM_{2.5}
 213 in Chengdu was much higher than the annual secondary guideline value (35 μg/m³,
 214 Ambient air quality standards/GB3095-2012) and the World Health Organization
 215 annual guideline value (10 μg/m³). The same PM_{2.5} pollution problem was also a
 216 serious problem in Beijing and Nanjing (Ji et al., 2019; Zheng et al., 2019). The annual

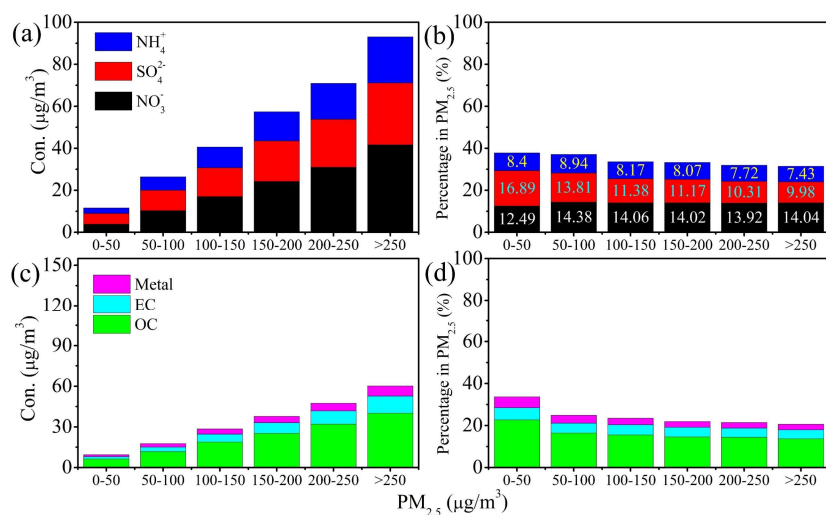
217 average mass concentration of NSA also changed significantly, and the difference was
218 large. The Mann-Whitney U test showed that the variation in NO_3^- was nonsignificant
219 ($p > 0.05$), and SO_4^{2-} and NH_4^+ had obvious significance from 2015 to 2017 ($p < 0.05$),
220 indicating that NO_3^- had not decreased significantly, and there was an increase in 2017
221 compared to 2015. SO_4^{2-} continued to decline, and NH_4^+ was also lower in 2017 than
222 in 2016. Notably, SO_4^{2-} and NH_4^+ decreased significantly in 2017 compared with 2015,
223 but the variation in NO_3^- was nonsignificant. Meanwhile, the annual averages of NO_3^-
224 / SO_4^{2-} were 0.95, 1.02 and 1.45 for 2015, 2016 and 2017, respectively, indicating that
225 the contribution of NO_x emissions sources to $\text{PM}_{2.5}$ was increased compared with that
226 of SO_2 emissions sources (Li et al., 2017; Wang et al., 2015). As shown in Table S1,
227 from 2013 to 2017, the emissions of NO_2 in Chengdu were obviously higher than those
228 of SO_2 , but $\text{PM}_{2.5}$, NO_2 and SO_2 all decreased due to the implementation of the Air
229 Pollution Prevention and Control Action Plan launched by the Chinese government and
230 a more detailed pollution control plan launched by Sichuan Province. From 2015 to
231 2017, the measures taken by Sichuan Province in the coordinated reduction of multiple
232 pollutants have been continuously strengthened, and the scope of management and
233 control has been continuously expanded, for example, in the improvement of
234 desulfurization, denitrification and dust removal technologies in key industries, from
235 accelerated improvement in 2015 to deeper improvement in 2017. The process of
236 eliminating small coal-fired boilers began in 2015 and was completed in 2017, when
237 the ultra-low-emission coal-fired power plant transformation was promoted. In terms
238 of vehicle emission control, we accelerated the elimination of "yellow label" vehicles
239 (general term for gasoline vehicles with emission levels lower than the national I
240 emission standard and diesel vehicles with emission levels lower than the national III
241 emission standard when new vehicles are finalized) and "old vehicles" (the emission
242 level does not meet the national stage IV emission standard) in 2015 and basically
243 completed the elimination of "yellow label" vehicles in 2017. The quality supervision
244 of oil products has also been improved, and non-road mobile machinery pollution

245 control requirements were proposed in the 2017 plan (The People's Government of
 246 Sichuan Province, 2015, 2016, 2017, last access: June 17, 2020). Compared with 2015,
 247 NO_x and SO₂ decreased by 5.98% and 32.35%, respectively, in 2017, which shows that
 248 the treatment of NO_x and SO₂ emissions has achieved remarkable results, of which the
 249 SO₂ emission reduction effect is the best, followed by that of NO_x. The effect of this
 250 emission reduction is due to air pollution prevention measures, especially measures of
 251 "electricity instead of coal" and "natural gas instead of coal" (refers to increased use of
 252 electricity and natural gas in the residential sector to reduce coal combustion).

253 Table 2. Comparison of annual mass averages ($\mu\text{g}/\text{m}^3$) and proportions (%) for NSA
 254 (nitrate, sulfate and ammonium) from 2015 to 2017.

	PM _{2.5}	SO ₄ ²⁻	NH ₄ ⁺	NO ₃ ⁻	NO ₃ ⁻ /PM _{2.5}	SO ₄ ²⁻ /PM _{2.5}	NH ₄ ⁺ /PM _{2.5}
2015	67.78	10.37	6.14	9.13	0.129	0.165	0.088
2016	71.88	8.53	6.16	9.27	0.123	0.133	0.089
2017	59.68	6.88	5.01	9.17	0.141	0.132	0.079

255



256

257 Fig. 2. Variation characteristics of the NSA (nitrate, sulfate and ammonium) and other

258 chemical compositions with different concentrations of PM_{2.5}. (a) NSA mass

259 concentration. (b) Percentage of NSA in $PM_{2.5}$. (c) Chemical compositions of organic
260 carbon (OC), elemental carbon (EC), and metal elements. (d) Percentage of OC, EC
261 and metal elements in $PM_{2.5}$.

262 The chemical compositions of $PM_{2.5}$ from 2015 to 2017 varies with concentration, as
263 shown in Fig. 2. With the accumulation of $PM_{2.5}$ in the atmosphere, the concentration
264 of NSA also increased significantly, but the proportion of NSA in $PM_{2.5}$ decreased (Fig.
265 2a and b). The variation trend of OC, EC and metal elements with increasing $PM_{2.5}$
266 concentration is similar to that of NSA (Fig. 2c and d), and this variation trend of OC
267 and EC is consistent with the results of long-term observation research carried out in
268 Beijing (Ji et al., 2019). With the accumulation of $PM_{2.5}$ concentration, NSA, OC, EC
269 and metal element concentrations have an increasing trend, but their ratio with $PM_{2.5}$
270 gradually decreases, indicating that other compositions have a higher contribution. This
271 result, on the one hand, maybe since some chemical compositions such as ions and dust
272 have not included in the statistics, on the other hand, the unknown component may also
273 have a high contribution characteristic to $PM_{2.5}$ (Zhang et al., 2015;Huang et al., 2014).
274 For the contribution characteristics of unknown components of $PM_{2.5}$, studies in some
275 regions of China show that the contribution of higher $PM_{2.5}$ concentration is higher than
276 that of lower $PM_{2.5}$ concentration (Huang et al., 2014;Li et al., 2017;Geng et al., 2019).
277 The chemical composition of $PM_{2.5}$ from 2015 to 2017 varies with concentration, as shown
278 in Fig. 2. With the accumulation of $PM_{2.5}$ in the atmosphere, the concentration of NSA also
279 increased significantly, but the proportion of NSA in $PM_{2.5}$ decreased (Fig. 2a and b). This
280 phenomenon occurs because some chemical components are included in the statistical
281 analysis. It also reflects that the chemical components of $PM_{2.5}$ have more complex
282 characteristics when pollution is aggravated. Some studies have analysed the changes in
283 the chemical composition of particulate matter in regions with severe pollution in China in
284 recent years, and the results show that the concentration of particulate matter has been
285 significantly reduced, but other components (except NSA and carbonaceous aerosol) have
286 higher contribution characteristics at higher particle concentrations (Geng et al.,

287 ~~2019; Wang et al., 2019). The variation trend of OC, EC and metal elements with increasing~~
288 ~~PM_{2.5} concentration is similar to that of NSA (Fig. 2e), and this variation trend of OC and~~
289 ~~EC is consistent with the results of long term observation research carried out in Beijing~~
290 ~~(Ji et al., 2019).~~ When PM_{2.5} was less than 50 µg/m³ and greater than 250 µg/m³, the
291 mass concentrations of NSA were 11.57 and 90.06 µg/m³, respectively, and the
292 proportions were 37.78 and 31.45%, respectively. Comparing Fig. 2b and d, it was
293 found that NSA was always the main contributor in the entire process of PM_{2.5}
294 accumulation, which was significantly higher than the proportions of OC and EC (Ji et
295 al., 2019; Li et al., 2019b). In the accumulation process of PM_{2.5} concentrations greater
296 than 50 µg/m³, NO₃⁻ accounts for a high proportion in NSA and is stable at
297 approximately 14%, and the proportion of SO₄²⁻ and NH₄⁺ continues to decrease (Li et
298 al., 2019b; Wang et al., 2016). When the PM_{2.5} concentration was less than 50 µg/m³,
299 the concentration of SO₄²⁻ was higher than that of NO₃⁻, and the concentration of NH₄⁺
300 was lower than the NH₄⁺ concentration of PM_{2.5} at 50 to 100 µg/m³, possibly due to
301 SO₄²⁻ concentration being higher than the NO₃⁻ concentration, forming more chemically
302 stable (NH₄)₂SO₄ (Guo et al., 2017a). In addition, when the PM_{2.5} was less than 50
303 µg/m³, low RH and strong solar radiation were also important ways to generate sulfate
304 (Yao et al., 2018).

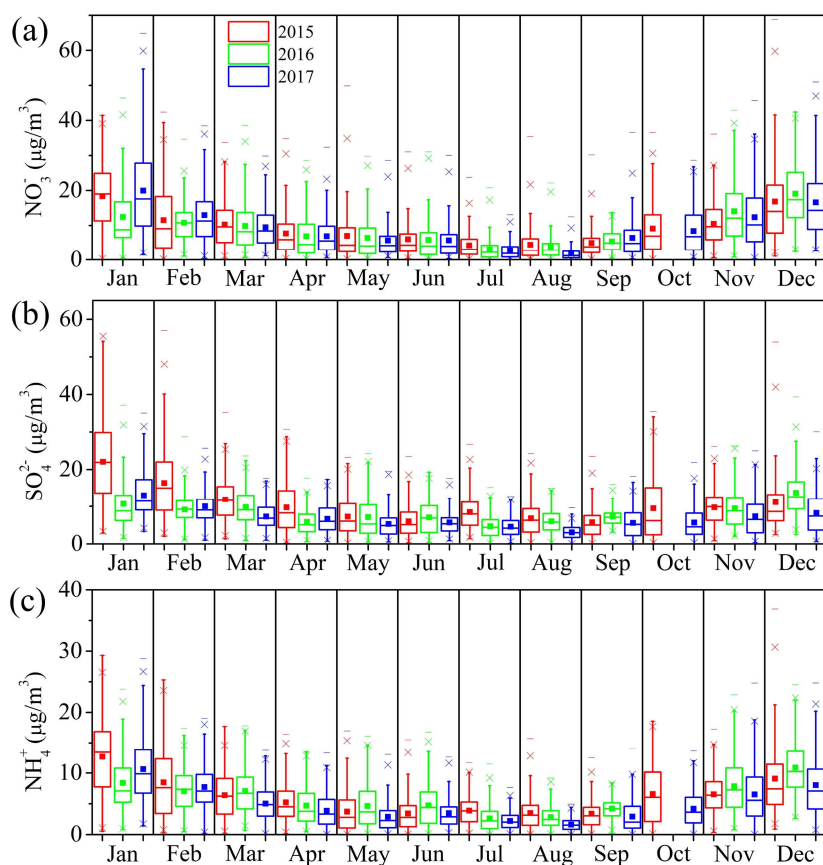
305 **3.2 Monthly and seasonal variations**

306 The monthly variation characteristics of NSA from 2015 to 2017 are shown in Fig. 3.
307 At the beginning and end of each year, the pollutant concentration is relatively high and
308 relatively low in the middle of each year. The meteorological conditions also have
309 obvious monthly variation characteristics (Fig. S5 a and b); from April to August, they
310 have higher WS and lower RH, which is not only conducive to the dilution and diffusion
311 of pollutants but also reduces the chemical conversions of pollutants by aqueous phase
312 and influences the formation of secondary inorganic aerosols (Wang et al., 2016; Ji et
313 al., 2019). Overall, the concentrations are higher in January and December and lower
314 in July and August. The highest monthly average NO₃⁻ reached 19.98 µg/m³ in January

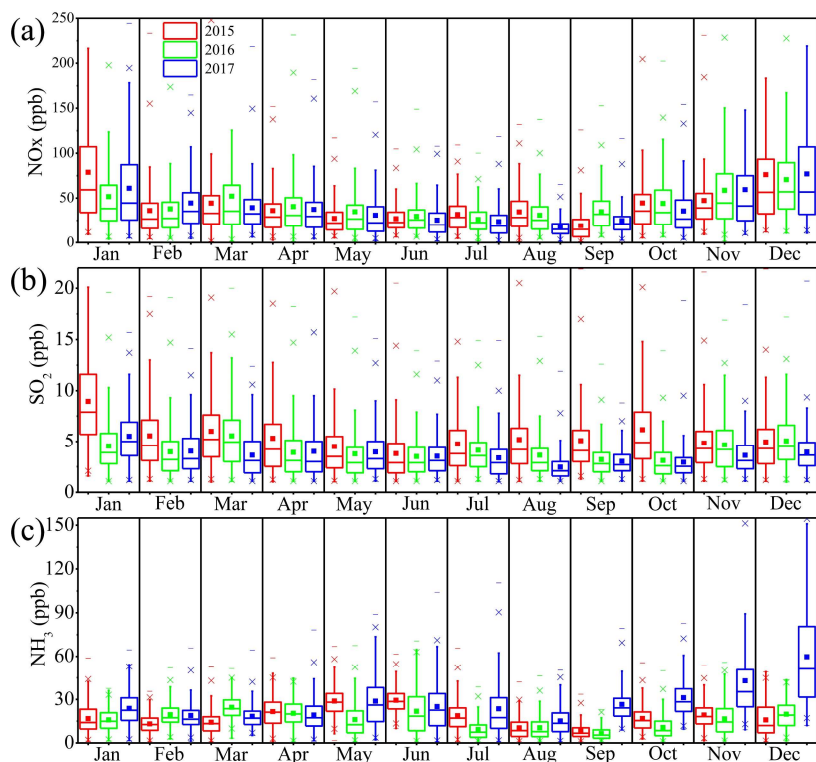
315 2017, and the highest monthly average SO_4^{2-} and NH_4^+ were $22.08 \mu\text{g}/\text{m}^3$ and 12.66
316 $\mu\text{g}/\text{m}^3$ in January 2015, respectively. The lowest concentrations of NSA appeared in
317 August 2017, which were 1.96, 3.07 and $1.62 \mu\text{g}/\text{m}^3$. The gaseous precursors of NSA
318 also have obvious monthly variations, and the NO_x and SO_2 trends were similar to those
319 of NO_3^- and SO_4^{2-} (Fig. 3 and 4). NH_3 emissions were significantly different, with
320 increases in warmer months (April-July) and colder months (September-December).
321 On the one hand, NH_3 volatilization was promoted by relatively high T_s (Fig. S5c); on
322 the other hand, the use of agricultural fertilizers and livestock farming were also
323 important sources of NH_3 in China. Second, from urban region, fossil fuel combustion
324 and motor vehicle emissions also contribute significantly (Liu et al., 2013b; Pan et al.,
325 2016). Notably, NH_3 increased significantly from April to December 2017 compared
326 with 2015 and 2016, especially during low- T months (Fig. 4c). The results of an
327 analysis of the monthly concentration variation of pollutants indicate that the
328 implementation of pollution reduction and control measures should be strengthened at
329 the beginning of each year (January to March) and the end of the year (October to
330 December).

331 The seasonal variation in NSA is shown in Fig. S6, and the concentration in winter was
332 much higher than that in summer. NO_3^- only declined in spring and summer from 2015
333 to 2017, with an increase in autumn and winter (Fig. S6a). Seasonal variations in NH_4^+
334 were similar to those of NO_3^- , with higher concentrations in winter and the lowest in
335 summer (Fig. S6c). This may be because higher T_s and WS_s can not only promote the
336 decomposition of NH_4NO_3 in summer but also promote the dilution and diffusion of
337 pollutant concentrations (Guo et al., 2017a; An et al., 2019). There is a significant
338 downward trend in SO_4^{2-} , which continues to decrease in spring, summer and winter
339 from 2015 to 2017 (Fig. S6b). In autumn, the concentration was the highest in 2016,
340 and it was significantly lower in 2017 than in 2015 and 2016. The variation amplitude
341 of NSA and gaseous pollutants in cold months was significantly higher than that in
342 warm months (Figs. 3, 4 and S6). This higher variation amplitude may be due to the

343 differences in pollutant accumulation and scavenging processes. This finding also
 344 indicates that the instability of local pollutant emissions and regional transport during
 345 cold months was affected by meteorological conditions (Li et al., 2017; Ji et al., 2018).
 346 The large variation amplitude of pollutants in different months, similar to the changes
 347 in the Beijing-Tianjin-Hebei region of northern China and Chengdu, are due to the
 348 accumulation and removal of pollution by meteorological conditions and pollutant
 349 emissions (Ji et al., 2019; Qin et al., 2019; Zhang et al., 2019a).



350
 351 Fig. 3. Monthly variations in NSA (nitrate, sulfate and ammonium) concentrations from
 352 2015 to 2017. (a) NO₃⁻. (b) SO₄²⁻. (c) NH₄⁺.



353

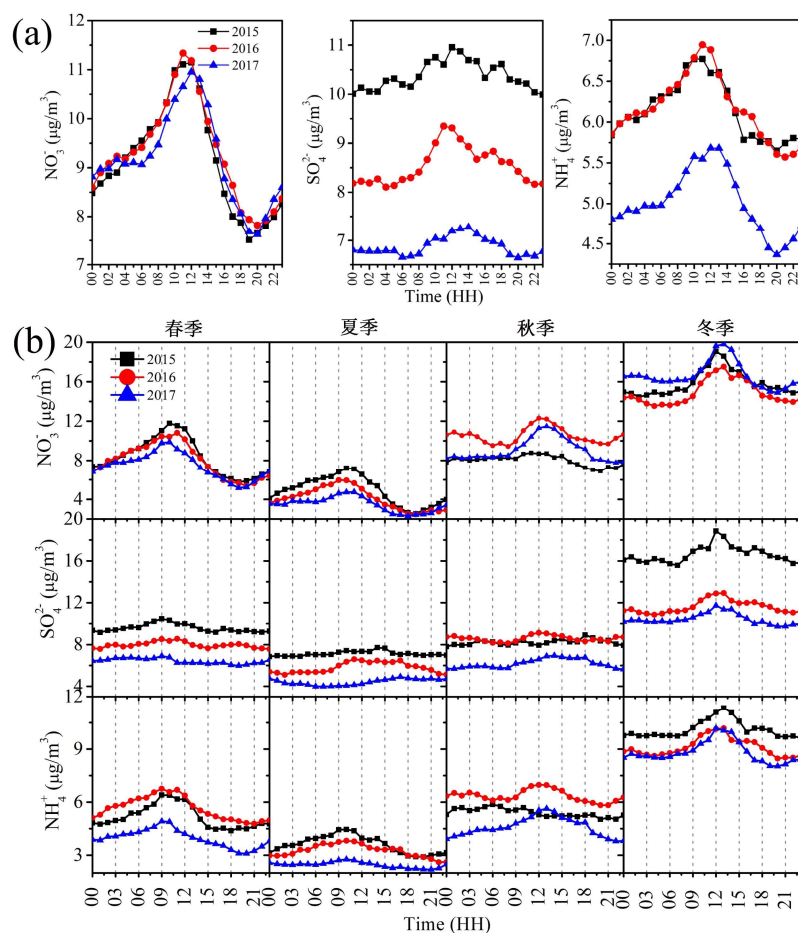
354 Fig. 4. Monthly variations in NO_x, SO₂ and NH₃ concentrations from 2015 to 2017. (a)
 355 NO_x. (b) SO₂. (c) NH₃.

356 3.3 Diurnal and weekly variations

357 From 2015 to 2017, the concentration of NSA was higher in the daytime than in the
 358 evening (Fig. 5a), and similar results were found in different seasons (Fig. 5b), which
 359 may be due to the combination of pollutant emissions and meteorological conditions.
 360 As shown in Fig. S7, from 9:00 to 11:00 a.m., the concentrations of SO₂, NO_x, NH₃
 361 and CO increased significantly, indicating that the primary emission of pollutants was
 362 relatively strong. At this time, although RH is in a declining stage, it still has a relatively
 363 high atmospheric humidity (approximately 65%), and O₃ and NO₂/NO also
 364 occasionally show an increasing trend, indicating that the atmospheric oxidizability has
 365 also increased (Figs. S7 and S8). This situation also provides favourable conditions for

366 the formation of secondary aerosols and promotes the accumulation of NSA (Cheng et
367 al., 2016; Wang et al., 2016; Sun et al., 2014). In addition, before 10 o'clock, relatively
368 low WS will enable easy pollutant concentration accumulation. In contrast, the higher
369 WS in the afternoon may be the main factor for the decrease in pollutant concentration
370 (Figs. 5 and S8). Photochemical reactions may also be one of the factors in the
371 formation of NSA, and the concentration of O₃ peaks at approximately 15:00, which
372 may be affected by the free radicals generated by photochemistry. At approximately
373 19:00, the ratio of NO₂/NO reached its highest value, and the concentration of NO₂ also
374 increased significantly (Song et al., 2018; Zhu et al., 2019). At night, with the increase
375 in RH (Fig. S8), dissolved ozone, free radicals, hydrogen peroxide and NO₂ can catalyse
376 SO₂ to form secondary aerosols through an aqueous phase reaction (Zhang et al.,
377 2015; An et al., 2019). The seasonal diurnal variation in NSA is shown in Fig. 5b. The
378 concentration of NSA in winter was obviously higher than that in summer, and the
379 diurnal variation range was larger. The concentrations in spring and autumn were closer,
380 but the diurnal variation in spring was larger than that in autumn. The larger diurnal
381 variation range not only indicates serious pollution but also indicates the importance of
382 other factors affecting air quality, such as meteorological conditions and secondary
383 aerosol conversion conditions (Ji et al., 2019; Yang et al., 2015b). The peak value of the
384 NSA seasonal diurnal variation also varies in different seasons. The peak value appears
385 at approximately 13:00 in winter, approximately 10:00 in spring and summer, and
386 approximately 12:00 in autumn, possibly due to the influence of meteorological
387 conditions. In previous studies in Beijing-Tianjin-Hebei and the Pearl River Delta, the
388 concentration of pollutants was affected by meteorological factors, and it was usually
389 lower in the daytime than at night. In the Yangtze River Delta, the peak usually occurs
390 in the morning, but in our study, the concentration was higher in the daytime than at
391 night (Peng et al., 2011; Wang et al., 2018; Guo et al., 2017b). In addition to the diurnal
392 variations in WS and atmospheric humidity, some studies have shown that due to the
393 unique topographical structure of the Sichuan Basin, the atmospheric circulation

394 between the Qinghai-Tibet Plateau, Yunnan-Guizhou Plateau and Sichuan Basin and
 395 the meteorological conditions of the Chengdu region are affected, such as the
 396 characteristics of air mass transport and typical “night rain” (more precipitation at night
 397 than in the day) under the influence of atmospheric circulation (Zhang et al.,
 398 2019c; Zhang et al., 2019b).



399
 400 Fig. 5. Diurnal variations in NSA (nitrate, sulfate and ammonium) from 2015 to 2017.
 401 (a) Annual average. (b) Seasonal average.

402 The weekly variation in NSA is shown in Fig. S9. During the overall observational
 403 period, workdays (Monday to Friday) showed higher variations than weekends

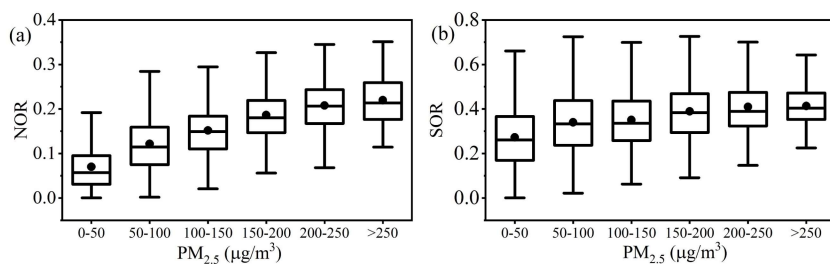
404 (Saturday and Sunday), with the highest variation being on Tuesday and the lowest
405 being on Sunday. Despite the difference in mean values between Tuesday and Sunday,
406 nonparametric tests show that the difference in mean values was nonsignificant (Mann-
407 Whitney U test, $P > 0.05$). As shown in Fig. S9, the average trends of NO_3^- and NH_4^+
408 were consistent from Monday to Sunday. The correlation coefficient was 0.94 ($P < 0.01$)
409 from 2015 to 2017, which indicates that they have a common source and that vehicle
410 emissions also have an important contribution to NH_4^+ (Pan et al., 2016). The average
411 NO_3^- , SO_4^{2-} and NH_4^+ concentrations from 2015 to 2017 were 9.21, 8.64 and 5.64 $\mu\text{g}/\text{m}^3$
412 on workdays and 8.56, 8.33 and 5.29 $\mu\text{g}/\text{m}^3$ on weekends, respectively. The average
413 values of NO_x , SO_2 and NH_3 were 42.43, 4.35 and 20.39 ppb on weekdays and 39.60,
414 4.34 and 19.67 ppb on weekends, respectively. Similarly, the mean difference between
415 NSA and gaseous precursors (NO_x , SO_2 and NH_3) was not significant by the Mann-
416 Whitney U test on weekdays and weekends. Population standard deviation comparisons
417 of NO_3^- , SO_4^{2-} and NH_4^+ showed that workdays had higher standard deviations than did
418 weekends, with 7.96, 6.04 and 4.35 on weekdays and 6.76, 5.69 and 3.88 on weekends,
419 respectively, and it could also be seen from the box chart of NSA weekly variation that
420 the concentration range on working days was slightly larger than that on weekends (Fig.
421 S10). Analysis of the diurnal variation in NSA gaseous precursors on weekdays and
422 weekends shows that the variation trend is relatively consistent (Fig. S11), and the
423 concentration of NO_x on weekdays will be slightly higher at the peak of 9:00 to 10:00
424 than on weekends, which may be affected by the morning rush hour of vehicles. In this
425 study, NSA and gaseous precursors are also slightly higher on weekdays than on
426 weekends, which indicates that in Chengdu's air pollution prevention and control
427 actions, the management of relevant industries and departments should be strengthened
428 on weekdays.

429 3.4 Chemical characteristics of NSA

430 3.4.1 Chemical conversion characteristics of NSA

431 Fig. 6 shows the abilities of NO_2 and SO_2 to chemically convert to NO_3^- and SO_4^{2-} at

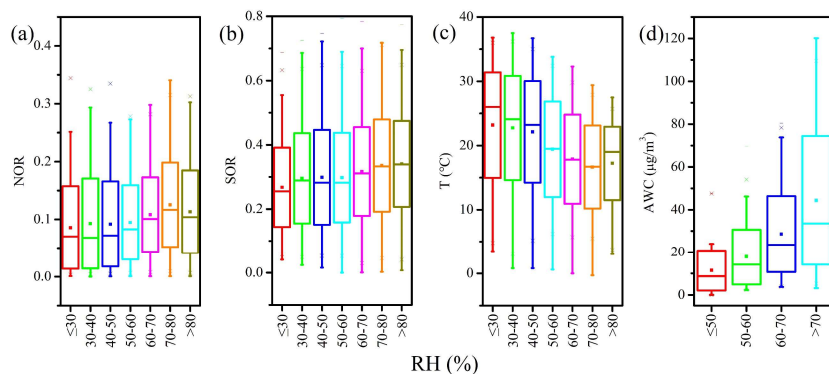
432 different $PM_{2.5}$ concentrations. With the increase in $PM_{2.5}$ concentration, NOR and SOR
 433 gradually increased, indicating that the formation ability of NO_3^- and SO_4^{2-} increased
 434 during the formation of air pollution. In this study, when the $PM_{2.5}$ concentration was \leq
 435 $50 \mu\text{g}/\text{m}^3$, the average NOR and SOR were 0.07 and 0.27, respectively, and when the
 436 $PM_{2.5}$ concentration was greater than $250 \mu\text{g}/\text{m}^3$, the average NOR and SOR increased
 437 to 0.22 and 0.41, respectively, indicating that the chemical conversion and formation
 438 ability of secondary inorganic aerosols was obviously enhanced when air pollution was
 439 aggravated. Previous studies suggested that when NOR and SOR were greater than 0.1
 440 and 0.2, respectively, it has intense conversions and forms secondary inorganic aerosols
 441 (Yang et al., 2015a).



442
 443 Fig. 6. Analysis of atmospheric chemical conversion ability at different $PM_{2.5}$
 444 concentrations. (a) NOR (nitrogen oxidation ratio). (b) SOR (sulfur oxidation ratio).

445 Fig. 7 shows the variation characteristics of NSA chemical conversions with increasing
 446 RH. NOR and SOR increased with increasing RH, suggesting that NO_2 and SO_2 were
 447 more likely to produce NO_3^- and SO_4^{2-} under higher RH conditions. Previous studies
 448 have shown that the presence of NH_3 and NO_2 can promote the chemical conversion of
 449 SO_2 to SO_4^{2-} in the aqueous phase (Wang et al., 2016). In an aerosol aqueous phase
 450 environment, alkaline aerosol (NH_3) components can promote the dissolution of SO_2
 451 and the formation of SO_4^{2-} under the oxidation of NO_2 (Cheng et al., 2016). Especially
 452 when the atmosphere is polluted, the formation of SO_4^{2-} by SO_2 through the aqueous
 453 phase environment can contribute most of the SO_4^{2-} (Sun et al., 2013). When the RH is
 454 greater than 80%, the NOR appears to decline, possibly because HNO_3 is semivolatile,

455 and the T increases at this time (Fig. 7 c), which is not conducive to the condensation
 456 of gaseous HNO₃ to particulate matter, which affects the amount of NO₃⁻ in PM_{2.5} (Guo
 457 et al., 2017a). According to the ISORROPIA-II thermodynamic equilibrium model
 458 simulation, AWC also increases with RH (Fig. 7 d), and the increase in AWC can
 459 provide a liquid environment for aerosols, which is conducive to the dissolution and
 460 conversion of gaseous precursors of NO₂, SO₂ and NH₃ and promotes the formation of
 461 more NSA. The Pearson's correlation coefficients of RH and NOR and SOR were 0.12
 462 and 0.16 (p<0.01), and the AWC and NOR and SOR were 0.73 and 0.37 (p<0.01),
 463 respectively, showing a significant positive correlation, indicating that the increase in
 464 AWC may be beneficial to the conversion of NO₂ and SO₂ to NO₃⁻ and SO₄²⁻. As shown
 465 in Fig. S12, the simulated values of NSA (metastable state, liquid phase components)
 466 are compared with the observed data. The linear regression fitting slope is
 467 approximately 1 (p<0.01), indicating that the effect of the liquid phase environment in
 468 PM_{2.5} is obvious; in addition, stable state simulation is also performed, and the linear
 469 regression fitting slopes of the NSA liquid phase state data output from the model and
 470 the observation data are 0.73, 0.63 and 0.74, and the Pearson's correlations are 0.82,
 471 0.71 and 0.80 (p<0.01), indicating that they are more often combined with AWC in the
 472 aerosol aqueous phase environment at a stable state. Previous studies have also
 473 confirmed that the aqueous phase environment of aerosols plays an important role in
 474 the formation of secondary inorganic aerosols (Wang et al., 2016; Cheng et al., 2016).



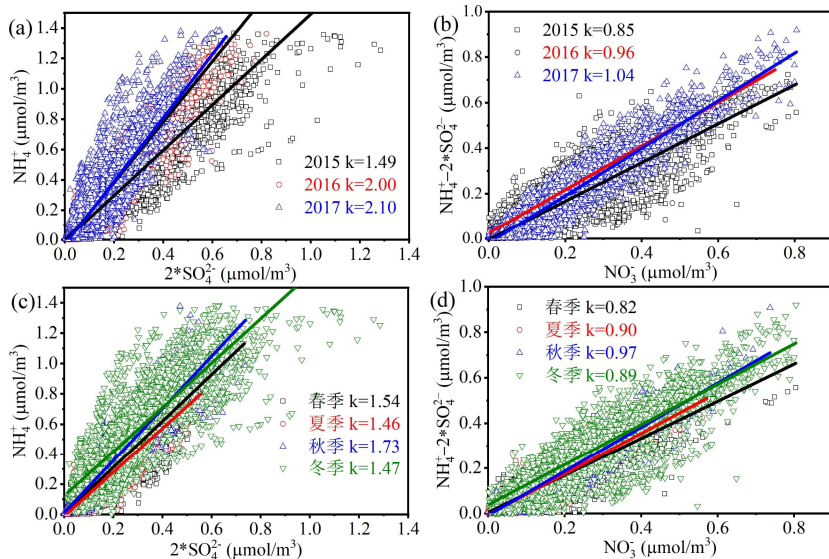
475

RH (%)

476 Fig. 7. Effects of RH on the chemical conversion of NSA (nitrate, sulfate and
477 ammonium). (a) NOR (nitrogen oxidation ratio). (b) SOR (sulfur oxidation ratio). (c)
478 Temperature (T). (d) AWC (aerosol water content).

479 3.4.2 Sensitivity analysis

480 The molar ratio analysis of NSA shown in Fig. 8 was used to analyse the chemical
481 relationships among NSA. $(\text{NH}_4)_2\text{SO}_4$ and NH_4NO_3 are mainly composed of NH_4^+ ,
482 SO_4^{2-} and NO_3^- in particulate matter (Malm and Hand, 2007; Meier et al., 2009).
483 Because $(\text{NH}_4)_2\text{SO}_4$ has better stability than NH_4NO_3 , NH_4^+ will first combine with
484 SO_4^{2-} and then with NO_3^- (Liu et al., 2012). The annual average molar ratio of NH_4^+ to
485 $2*\text{SO}_4^{2-}$ was more than 1, which indicates that SO_4^{2-} can be completely neutralized by
486 NH_4^+ (Fig. 8a). The molar ratios of residual NH_4^+ ($\text{NH}_4^+ - 2*\text{SO}_4^{2-}$) to NO_3^- were 0.85,
487 0.96 and 1.04 in 2015, 2016 and 2017, respectively. As shown in Fig. 8a and b, the
488 gradual increase in the ratio (slope k) from 2015 to 2017 indicates that there is an
489 increase in NH_4^+ in aerosol compared with SO_4^{2-} and NO_3^- , especially in 2017, with a
490 ratio of 1.04, indicating the presence of other forms of NH_4^+ , such as NH_4Cl and
491 $(\text{NH}_4)_2\text{C}_2\text{O}_4$ (Sun et al., 2006). Seasonal variations in NH_4^+ , SO_4^{2-} and NO_3^- are shown
492 in Fig. 8c and d. The higher molar ratio in autumn indicates that the intensity of
493 ammonia emission in autumn was higher than that in other seasons. This result also
494 shows that the proportion of NH_4^+ relative to NO_3^- and SO_4^{2-} in $\text{PM}_{2.5}$ has increased.
495 Therefore, while currently controlling NO_x and SO_2 emissions, it is also necessary to
496 strengthen NH_3 emissions control.



497

498 Fig. 8. Molar ratio analysis of NSA (nitrate, sulfate and ammonium). (a) Interannual
 499 variation in the molar ratio of SO_4^{2-} and NH_4^+ . (b) Interannual variation in the molar
 500 ratio of NO_3^- and NH_4^+ . (c) Seasonal variation in the molar ratio of SO_4^{2-} and NH_4^+ . (d)
 501 Seasonal variation in the molar ratio of NO_3^- and NH_4^+ . k: Fitting slope of linear
 502 regression.

503 Table 3 shows the sensitivity analysis of the concentration variations in SO_4^{2-} , NO_3^- and
 504 NH_4^+ . ISORROPIA-II thermodynamic equilibrium model sensitivity analysis is
 505 described in detail in the Supplementary Materials. The coefficient of variance
 506 represents the response of the species to variations in other components. The
 507 coefficients of variance for NH_4^+ and NO_3^- produced by SO_4^{2-} changes were 52.22 and
 508 1.70, respectively. Similarly, the coefficients of variance for NH_4^+ and SO_4^{2-} produced
 509 by NO_3^- changes were 51.42 and 0.0005, respectively. The large coefficient of variance
 510 for NH_4^+ indicates that the changes in NO_3^- and SO_4^{2-} can affect the presence of NH_4^+ ,
 511 which also indicates that NH_4NO_3 and $(\text{NH}_4)_2\text{SO}_4$ were the main states of NH_4^+ (Liu et
 512 al., 2012). The coefficients of variance for SO_4^{2-} and NO_3^- produced by TNH_3
 513 ($\text{NH}_3+\text{NH}_4^+$) changes were 0.47 and 15.76, respectively, and the effect of TNH_3 on

514 SO_4^{2-} was less than that of NO_3^- , which indicates that NH_4^+ was excessive to SO_4^{2-} and
 515 that NH_4^+ first combines with SO_4^{2-} to form stable $(\text{NH}_4)_2\text{SO}_4$, and the remaining NH_4^+
 516 and NO_3^- will combine to form NH_4NO_3 .

517 Table 3. Sensitivity analysis of NSA (nitrate, sulfate and ammonium) concentration
 518 variations during the different observation periods.

Period	Variation	Coefficients of variance		
		NO_3^-	NH_4^+	SO_4^{2-}
2015-2017	NO_3^-		51.42	0.0005
	TNH_3	15.76		0.47
	SO_4^{2-}	1.70	52.22	

Coefficients of variance: standard deviation/average *100%;

Variation TNH_3 : $\text{NH}_3+\text{NH}_4^+$ ($\mu\text{g}/\text{m}^3$);

Variation SO_4^{2-} and NO_3^- units: $\mu\text{g}/\text{m}^3$

519 Through the implementation of the Air Pollution Prevention and Control Action Plan,
 520 the reduction in SO_4^{2-} in $\text{PM}_{2.5}$ has achieved good results. Therefore, while continuing
 521 to promote "electricity instead of coal" and "natural gas instead of coal" to reduce coal
 522 combustion pollution, more stringent control measures should be added for NO_3^- and
 523 NH_4^+ emissions. To further improve air quality, the Chinese government launched a
 524 "Three-Year Action Plan for Winning the Blue Sky Defense Battle" in 2018 and
 525 proposed emission reduction targets for NO_x and SO_2 emissions, which will be 15%
 526 lower in 2020 than in 2015 (the State Council, 2018, last access: June 17, 2020). The
 527 results of using the ISORROPIA-II thermodynamic equilibrium model to simulate NO_3^- ,
 528 SO_4^{2-} and TNH_3 emission reduction control effects of 5%, 10%, 15% and 20%,
 529 respectively, are shown in Table S3, showing that controlling the concentration of NO_3^-
 530 and SO_4^{2-} is also helpful to reduce the concentration of NH_4^+ and indicating that
 531 controlling its precursor NO_x and SO_2 is of great significance to reduce the secondary
 532 inorganic aerosol in $\text{PM}_{2.5}$ (the detailed results are described in the supplementary
 533 materials). Previous studies have also shown that the conversion of SO_2 to SO_4^{2-} in the

534 aqueous phase not only increases the conversion of SO_4^{2-} but also enhances the
535 formation of NO_3^- in the aqueous phase (Wang et al., 2016). Therefore, SO_2 emission
536 reduction may play a key role in the process of controlling emission reduction in NSA
537 pollution, as it not only reduces the presence of NH_4^+ ($(\text{NH}_4)_2\text{SO}_4$) in particulate matter
538 but also affects the formation of NH_4NO_3 by influencing the formation of NO_3^- . NO_2
539 and NH_3 can also promote the conversion of SO_2 to SO_4^{2-} through an aqueous phase
540 environment (Wang et al., 2016). Therefore, priority control of NO_x and SO_2 emissions
541 is an important way to reduce NSA in particulate matter.

542 The increase in NSA can increase the hygroscopicity properties of aerosols, and more
543 AWC can increase the pH by diluting the hydrogen ion concentration (Kong et al.,
544 2020; Ding et al., 2019). Previous studies have also shown that SO_4^{2-} formation reduces
545 aerosol pH (Sun et al., 2014). The effects of NO_3^- , SO_4^{2-} and TNH_3 on pH when using
546 the ISORROPIA-II thermodynamic equilibrium model to simulate pollutant
547 concentration reduction are shown in Table S3. With the decrease in NO_3^- and SO_4^{2-} ,
548 the pH value increases, but NO_3^- has no obvious effect on the pH value, SO_4^{2-} has an
549 obvious effect on the pH value, which indicates that the formation of SO_4^{2-} in the
550 aerosol can increase the acidity of the aerosol (Sun et al., 2014). The greater the
551 reduction of TNH_3 , the lower the pH value is, which shows that the presence of NH_3 as
552 an alkaline gas can alleviate some of the acidity produced by SO_4^{2-} (Cheng et al., 2016).
553 When the synergistic control of pollutants is reduced, it also has a certain effect on pH,
554 increasing from 4.07 to 4.16. Some studies believe that if ammonia emissions are
555 reduced significantly, the risk of acid rain may increase (Liu et al., 2019c). As shown
556 in Fig. S13, the acid rain problem in China is mainly concentrated in southern China,
557 especially in southwestern China, southern China, and the Yangtze River Delta in
558 eastern China. Therefore, how to adjust the emission reduction ratio in combination
559 with the characteristics of regional air pollution and energy consumption and thus help
560 reduce the problem of aerosol acidity changes caused by air pollution reduction is a
561 problem worthy of in-depth study. Therefore, when controlling NO_x , SO_2 and NH_3

562 emissions, it is necessary to consider the aerosol acid and alkali changes caused by
563 emission reduction.

564 **3.5 Characteristics of local emissions and regional transport**

565 **3.5.1 Local emissions**

566 The concentration of pollutants is obviously affected by meteorological conditions; for
567 example, WS and WD can affect the accumulation and removal of pollutants (Li et al.,
568 2016). Figs. S14-16 show the annual variation characteristics of NSA and gas
569 precursors affected by the WS and WD using CPF. Overall, the higher WS was
570 accompanied by a lower pollutant concentration. As the WS decreased, the pollution
571 became serious, and the pollution hot spots were gradually concentrated. On the whole,
572 when the WS was usually greater than 2 m/s, the pollution was light (pollutant
573 concentration percentile was between 0-25). When WS was usually less than 1 m/s, the
574 pollution was heavy (pollutant concentration percentile was between 75-100), which
575 also reflects the distance and orientation between the emission source and the
576 observation station, indicating that when the pollution was serious, the contribution of
577 local source emissions was more prominent.

578 NO_3^- and NO_x have similar distributions of pollution hot spots in the polar plot diagram
579 (Fig. S14), and when the concentration percentile was 0-25, the hot spots were
580 concentrated in the northeast and southeast directions and widely distributed. When the
581 concentration percentile was 25-75, the sources of NO_3^- and NO_x were distributed west,
582 southwest and northeast of the observation site, and there were important contribution
583 sources in the northwest direction (WS was approximately 3-4 m/s) in 2017. When the
584 WS was approximately 1-2 m/s and the concentration percentile was 50-75, the
585 important NO_x source was in the northwest direction. When the accumulation of
586 pollution concentration was high (concentration percentile was 75-100), the NO_3^-
587 source was mainly concentrated in the east and southeast of the observation site, and
588 NO_x was distributed in the south and southeast, with WSs of less than 1 m/s.
589 Additionally, the distribution of pollution hot spots was relatively wide in 2016 (the

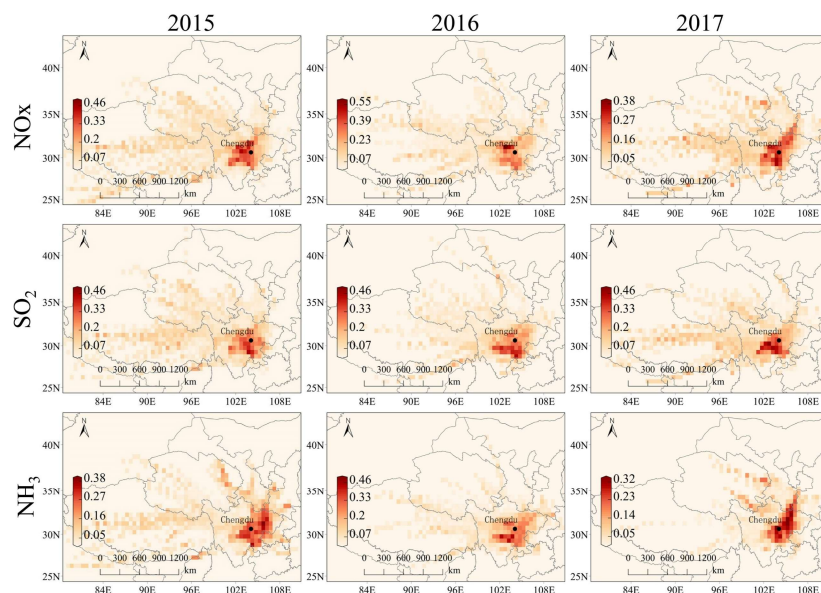
590 annual mean values of NO_x were 42.15, 43.99 and 39.63 ppb in 2015, 2016 and 2017,
591 respectively), indicating that the source was relatively wide, which may be one of the
592 reasons for the relatively high concentration. The SO₄²⁻ and SO₂ pollution sources
593 affected by meteorological conditions also have similar distribution characteristics (Fig.
594 S15). At a higher concentration of pollutants, the pollution hot spots of SO₄²⁻ were
595 distributed in the east and southeast of the observation site, and SO₂ was distributed in
596 the northeast, southeast and west. Compared with 2017 and 2016, the distribution of
597 SO₂ pollution sources in 2016 was also more extensive, mainly in the west and northeast.
598 The NH₃ emissions were slightly different from those of NO_x and SO₂ (Fig. S16).
599 Under conditions of high pollution concentration (concentration percentile was 75-100),
600 the pollution hot spots were distributed in the west in 2015 (WS was approximately 2-
601 3 m/s), in the north in 2016 (WS was approximately 1 and 3 m/s), and in the near
602 distance in 2017 (WS was approximately 0.5 m/s). The higher pollution concentration
603 was accompanied by a relatively higher WS (2015 and 2016), which indicates that the
604 NH₃ emission transport in the surrounding area was more obvious, which may come
605 from the surrounding agricultural source distribution area (Liu et al., 2019b; Liu et al.,
606 2013b). The annual mean value of NH₃ emissions in 2017 was 27.91 ppb, which is
607 significantly higher than those in 2015 and 2016 at 17.93 ppb and 16.55 ppb,
608 respectively. During the 25-50 concentration percentile period of NH₃, there was a WS
609 of approximately 2 m/s east of the observation site, and during the 50-75 concentration
610 percentile period, there was an obvious source northwest of the observation site, with a
611 WS of approximately 4 m/s. During the 75-100 concentration percentile periods, the
612 pollution sources were mainly local. This shows that in 2017, in addition to the pollution
613 sources being distributed in the east and northwest, the higher NH₃ emissions were also
614 contributed by the surrounding emission sources northwest of Chengdu.

615 **3.5.2 Gaseous precursors of NSA regional transport**

616 The PSCF is used to analyse the potential source distribution of pollutants to determine
617 the regional transport characteristics of pollutants (Ji et al., 2019). In addition,

618 considering the aerosol lifetime, SO₂ (approximately 9.6 d) and NO_x (approximately 1
619 d) are also very different (Guo et al., 2014), and the research also shows that NH₃ is
620 significantly contributed by local source emissions (Walker et al., 2004). Therefore, we
621 comprehensively consider selecting a 24-hour backward trajectory to carry out PSCF
622 simulation in the Chengdu region. Fig. 9 shows the PSCF analysis of NO_x, SO₂ and
623 NH₃, with significant differences in their potential source distributions. The higher
624 PSCF value of NO_x was mainly distributed west, northwest and southwest of Chengdu
625 in 2015, northwest and south of Chengdu in 2016, and south, west and northeast of
626 Chengdu in 2017. The PSCF of NO₂ and NO (Fig. S17) also reflects that their potential
627 sources are mainly influenced by the interior of Sichuan Province, especially in the
628 cities around Chengdu. Chengdu is located along the western margin of the Sichuan
629 Basin, and it was also observed through satellite remote sensing data that the higher
630 NO₂ emissions in the Sichuan Basin were distributed in Chengdu and Chongqing (Fig.
631 S18a). The SO₂ emissions were widely distributed, mainly in the Sichuan Basin. Among
632 them, Leshan city and Meishan city south of Chengdu had higher SO₂ emissions, and
633 another higher emission source was distributed in Chongqing (Fig. S18b). The PSCF
634 analysis of SO₂ showed that the higher PSCF values were distributed in southern,
635 western and southwestern Chengdu. Therefore, a comparison of Figs. 9 and S18b shows
636 that the main source of SO₂ may be distributed in the southern, western and
637 southwestern margin region of the Sichuan Basin. In particular, Leshan, Ya'an and
638 Meishan were important potential sources. As shown in the PSCF analysis of NH₃ in
639 Fig. 9, the higher PSCF was also concentrated in the inner Sichuan Basin, especially in
640 the urban agglomeration around Chengdu. In 2015, the potential source of NH₃ was
641 mainly distributed in the southwest and northeast of Chengdu, with higher PSCF in
642 Nanchong and other regions. In the southwest, it was concentrated in Ya'an, Meishan
643 and Leshan. In 2016, potential sources were mainly distributed in the southwest of Ya'an,
644 Meishan, Leshan and the southern part of the Ganzi Tibetan Autonomous Prefecture.
645 There were two characteristics of potential sources in 2017. A relatively light source

646 was relatively close to Chengdu, and the high PSCF was in Chengdu, which can be
647 considered the contribution of local emissions. The other contribution is obvious as a
648 long-distance potential source contribution, mainly in some cities in the northeast,
649 Nanchong, Guangyuan and Mianyang, and to a certain extent at the junction of Shaanxi,
650 Gansu and Sichuan. In 2017, in addition to the contribution of local emissions, the
651 contribution of regional transport in the northeast may also be an important reason for
652 the higher NH₃ concentration. Fig. S19 shows satellite remote sensing data of NH₃.
653 Overall, the higher NH₃ column concentration is distributed in the Sichuan Basin,
654 mainly concentrated in the region near Chengdu, showing that NH₃ is more discharged
655 in the Sichuan Basin, especially in the surrounding areas of Chengdu. In addition,
656 through the analysis of the Multiresolution Emission Inventory for China (MEIC), it is
657 also found that the higher NO_x, SO₂ and NH₃ emissions in Sichuan Basin are mainly
658 concentrated in Sichuan Basin, as shown in Fig. S20. It can also be seen that NO_x is
659 mainly concentrated in more-developed Chengdu and Chongqing, SO₂ emissions are
660 obvious in Chengdu and Western Chongqing, NH₃ emissions are widely distributed,
661 and there are higher emission characteristics in Chengdu and its surrounding areas.
662 Therefore, according to the analysis of pollution emissions and PSCF in Chengdu, it is
663 necessary to strengthen regional air pollution control and take regional joint prevention
664 and control measures to reduce the impact of air pollutant regional transport.



665

666 Fig. 9. PSCF (potential source contribution function) of NO_x, SO₂ and NH₃ in Chengdu
 667 from 2015 to 2017.

668 4 Conclusions

669 The three-year observation experiment with hourly resolution of NSA from January 1,
 670 2015 to December 31, 2017 was carried out in Chengdu in southwest China, which is
 671 in the Sichuan Basin. The pollution characteristics of NSA's annual, monthly, seasonal,
 672 diurnal and weekly variations were demonstrated. The characteristics of chemical
 673 conversion and the sensitivity of emission reduction control were analysed. Finally,
 674 combined with meteorological parameters and PSCF simulation, the local emission and
 675 regional transport characteristics of NSA gaseous precursors were also illustrated. The
 676 main conclusions were as follows:

677 (1) With the increase in PM_{2.5} concentration, the NSA mass concentration increased,
 678 accounting for 31.45-37.78% of PM_{2.5}, and the contribution of NSA was higher than
 679 that of carbon aerosol (OM and EC). From 2015 to 2017, the contribution of NO₃⁻ to
 680 PM_{2.5} increased, and in 2017, it became the main contribution component of NSA, and

681 it plays an important role in the concentration accumulation of $PM_{2.5}$. Higher and lower
682 NSA concentrations were seen in winter and summer, respectively, and higher
683 concentrations were seen more during the day than at night. Although the NSA
684 concentration on weekdays was slightly higher than that on weekends, the mean
685 difference between them was nonsignificant.

686 (2) With the increase in $PM_{2.5}$ concentration, there is an increasing trend of NOR and
687 SOR, which indicates that the formation of NO_3^- and SO_4^{2-} increases obviously, and the
688 increase in RH will promote the formation of NO_3^- and SO_4^{2-} . Using the ISORROPIA-
689 II thermodynamic equilibrium model, it is found that NSA in aerosols is more likely to
690 combine with AWC, which indicates that the aqueous environment of aerosols plays an
691 important role in promoting the formation of NSA. The analysis of the interaction
692 between NSA also confirmed that NH_4^+ will first combine with SO_4^{2-} to form
693 $(NH_4)_2SO_4$, and the remaining NH_4^+ will combine with NO_3^- to form NH_4NO_3 . The
694 sensitivity analysis of NSA concentration shows that reducing NO_x and SO_2 is
695 beneficial to reducing NSA contribution in $PM_{2.5}$, but their changes also have an
696 important impact on the pH of aerosols.

697 (3) Local emissions and regional transport of NSA gaseous precursors have an
698 important impact on air pollution in Chengdu. When pollution is aggravated, the
699 contributions of NO_x and SO_2 to local emissions are relatively obvious. In addition to
700 the local emission of NH_3 , the contribution of pollution sources around Chengdu is also
701 relatively obvious. PSCF analysis shows that the potential sources of pollution
702 transmission in Chengdu are mainly distributed in Sichuan Province, and the most
703 prominent contribution is made in Sichuan Basin, especially among the cities around
704 Chengdu. The analysis of local emissions and regional transport shows that it is
705 necessary to implement joint prevention and control of air pollution in the Sichuan
706 Basin.

707 **Acknowledgements**

708 This work was supported by the People's Republic of China Science and Technology

709 Department (No. 2018YFC0214001 and No. 2016YFC0202000) and the National
710 Natural Science Foundation of China (No. 91544221).

711 **Data availability**

712 The data are available on request to the corresponding author.

713 **Author contribution**

714 XL, QT and LK designed and led this study. QT and MF were responsible for the
715 observations. LK, MF, YL, YZ, CZ, and CL analysed the data. LK, YQ, JA, NC, YD,
716 RZ and ZW discussed the results. LK and XL wrote the paper. All authors commented
717 on the paper.

718 **Competing interests**

719 The authors declare that they have no conflicts of interest.

720 **References**

- 721 An, Z., Huang, R. J., Zhang, R., Tie, X., Li, G., Cao, J., Zhou, W., Shi, Z., Han, Y., Gu,
722 Z., and Ji, Y.: Severe haze in northern China: A synergy of anthropogenic
723 emissions and atmospheric processes, *Proceedings of the National Academy of*
724 *Sciences of the United States of America*, 116, 8657-8666,
725 10.1073/pnas.1900125116, 2019.
- 726 Beijing Municipal Ecology and Environment Bureau: Beijing Environmental Statement,
727 2018. Website: <http://sthjj.beijing.gov.cn/>, last access: June 17, 2020.
- 728 Chang, X., Wang, S., Zhao, B., Cai, S., and Hao, J.: Assessment of inter-city transport
729 of particulate matter in the Beijing-Tianjin-Hebei region, *Atmospheric*
730 *Chemistry and Physics*, 18, 4843-4858, 10.5194/acp-18-4843-2018, 2018.
- 731 Chen, L., Zhu, J., Liao, H., Gao, Y., Qiu, Y., Zhang, M., Liu, Z., Li, N., and Wang, Y.:
732 Assessing the formation and evolution mechanisms of severe haze pollution in
733 the Beijing-Tianjin-Hebei region using process analysis, *Atmospheric*
734 *Chemistry and Physics*, 19, 10845-10864, 10.5194/acp-19-10845-2019, 2019a.
- 735 Chen, Z., Chen, D., Wen, W., Zhuang, Y., Kwan, M., Chen, B., Zhao, B., Yang, L., Gao,
736 B., Li, R., and Xu, B.: Evaluating the "2+26" regional strategy for air quality
737 improvement during two air pollution alerts in Beijing: variations in PM_{2.5}
738 concentrations, source apportionment, and the relative contribution of local
739 emission and regional transport, *Atmospheric Chemistry and Physics*, 19, 6879-
740 6891, 10.5194/acp-19-6879-2019, 2019b.
- 741 Cheng, J., Su, J., Cui, T., Li, X., Dong, X., Sun, F., Yang, Y., Tong, D., Zheng, Y., Li,
742 Y., Li, J., Zhang, Q., and He, K.: Dominant role of emission reduction in PM_{2.5}
743 air quality improvement in Beijing during 2013–2017: a model-based
744 decomposition analysis, *Atmospheric Chemistry and Physics*, 19, 6125-6146,

745 10.5194/acp-19-6125-2019, 2019.

746 Cheng, Y., Zheng, G., Wei, C., Mu, Q., Zheng, B., Wang, Z., Gao, M., Zhang, Q., He,
747 K., Carmichael, G., Poschl, U., and Su, H.: Reactive nitrogen chemistry in
748 aerosol water as a source of sulfate during haze events in China, *Science*
749 *Advances*, 2, e1601530, 10.1126/sciadv.1601530, 2016.

750 Chengdu Municipal Ecology and Environment Bureau: Ambient air quality report,
751 2018. Website: <http://sthj.chengdu.gov.cn/>, last access: June 17, 2020.

752 Ding, J., Zhao, P., Su, J., Dong, Q., Du, X., and Zhang, Y.: Aerosol pH and its driving
753 factors in Beijing, *Atmospheric Chemistry and Physics*, 19, 7939-7954,
754 10.5194/acp-19-7939-2019, 2019.

755 Fountoukis, C., and Nenes, A.: ISORROPIA II: a computationally efficient
756 thermodynamic equilibrium model for K^+ - Ca^{2+} - Mg^{2+} - NH_4^+ - Na^+ - SO_4^{2-} - NO_3^- -
757 Cl^- - H_2O aerosols, *Atmospheric Chemistry and Physics*, 7, 4639-4659,
758 10.5194/acp-7-4639-2007, 2007.

759 Fountoukis, C., Nenes, A., Sullivan, A., Weber, R., Van Reken, T., Fischer, M., Matias,
760 E., Moya, M., Farmer, D., and Cohen, R. C.: Thermodynamic characterization
761 of Mexico City aerosol during MILAGRO 2006, *Atmospheric Chemistry and*
762 *Physics*, 9, 2141-2156, 10.5194/acp-9-2141-2009, 2009.

763 Fu, G., Xu, W., Yang, R., Li, J., and Zhao, C.: The distribution and trends of fog and
764 haze in the North China Plain over the past 30 years, *Atmospheric Chemistry*
765 *and Physics*, 14, 11949-11958, 10.5194/acp-14-11949-2014, 2014.

766 [Geng, G., Xiao, Q., Zheng, Y., Tong, D., Zhang, Y., Zhang, X., Zhang, Q., He, K., and](#)
767 [Liu, Y.: Impact of China's Air Pollution Prevention and Control Action Plan on](#)
768 [PM_{2.5} chemical composition over eastern China, *Science China Earth Sciences*,](#)
769 [62, 1872-1884, 10.1007/s11430-018-9353-x, 2019.](#)

770 Gui, K., Che, H., Wang, Y., Wang, H., Zhang, L., Zhao, H., Zheng, Y., Sun, T., and
771 Zhang, X.: Satellite-derived PM_{2.5} concentration trends over Eastern China
772 from 1998 to 2016: Relationships to emissions and meteorological parameters,
773 *Environmental Pollution*, 247, 1125-1133, 10.1016/j.envpol.2019.01.056, 2019.

774 Guo, H., Sullivan, A. P., Campuzano-Jost, P., Schroder, J. C., Lopez-Hilfiker, F. D.,
775 Dibb, J. E., Jimenez, J. L., Thornton, J. A., Brown, S. S., Nenes, A., and Weber,
776 R. J.: Fine particle pH and the partitioning of nitric acid during winter in the
777 northeastern United States, *Journal of Geophysical Research: Atmospheres*, 121,
778 10355-10376, 10.1002/2016jd025311, 2016.

779 Guo, H., Liu, J., Froyd, K. D., Roberts, J. M., Veres, P. R., Hayes, P. L., Jimenez, J. L.,
780 Nenes, A., and Weber, R. J.: Fine particle pH and gas-particle phase partitioning
781 of inorganic species in Pasadena, California, during the 2010 CalNex campaign,
782 *Atmospheric Chemistry and Physics*, 17, 5703-5719, 10.5194/acp-17-5703-
783 2017, 2017a.

784 Guo, J., Xia, F., Zhang, Y., Liu, H., Li, J., Lou, M., He, J., Yan, Y., Wang, F., Min, M.,
785 and Zhai, P.: Impact of diurnal variability and meteorological factors on the
786 PM_{2.5}-AOD relationship: Implications for PM_{2.5} remote sensing, *Environmental*

带格式的: 字体:(中文)+中文正文(等线)

787 pollution, 221, 94-104, 10.1016/j.envpol.2016.11.043, 2017b.

788 Guo, S., Hu, M., Zamora, M. L., Peng, J., Shang, D., Zheng, J., Du, Z., Wu, Z., Shao,
789 M., Zeng, L., Molina, M. J., and Zhang, R.: Elucidating severe urban haze
790 formation in China, *Proceedings of the National Academy of Sciences of the*
791 *United States of America*, 111, 17373-17378, 10.1073/pnas.1419604111, 2014.

792 He, H., Wang, Y., Ma, Q., Ma, J., Chu, B., Ji, D., Tang, G., Liu, C., Zhang, H., and Hao,
793 J.: Mineral dust and NO_x promote the conversion of SO₂ to sulfate in heavy
794 pollution days, *Scientific Reports*, 4, 4172, [10.1038/srep04172](https://doi.org/10.1038/srep04172), 2014.

795 [Huang, R. J., Zhang, Y., Bozzetti, C., Ho, K. F., Cao, J. J., Han, Y., Daellenbach, K. R.,
796 Slowik, J. G., Platt, S. M., Canonaco, F., Zotter, P., Wolf, R., Pieber, S. M., Bruns,
797 E. A., Crippa, M., Ciarelli, G., Piazzalunga, A., Schwikowski, M., Abbaszade,
798 G., Schnelle-Kreis, J., Zimmermann, R., An, Z., Szidat, S., Baltensperger, U.,
799 El Haddad, I., and Prevot, A. S.: High secondary aerosol contribution to
800 particulate pollution during haze events in China, *Nature*, 514, 218-222,
801 \[10.1038/nature13774\]\(https://doi.org/10.1038/nature13774\), 2014.](https://doi.org/10.1038/nature13774)

802 Ji, D., Yan, Y., Wang, Z., He, J., Liu, B., Sun, Y., Gao, M., Li, Y., Cao, W., Cui, Y., Hu,
803 B., Xin, J., Wang, L., Liu, Z., Tang, G., and Wang, Y.: Two-year continuous
804 measurements of carbonaceous aerosols in urban Beijing, China: Temporal
805 variations, characteristics and source analyses, *Chemosphere*, 200, 191-200,
806 10.1016/j.chemosphere.2018.02.067, 2018.

807 Ji, D., Gao, W., Maenhaut, W., He, J., Wang, Z., Li, J., Du, W., Wang, L., Sun, Y., Xin,
808 J., Hu, B., and Wang, Y.: Impact of air pollution control measures and regional
809 transport on carbonaceous aerosols in fine particulate matter in urban Beijing,
810 China: insights gained from long-term measurement, *Atmospheric Chemistry*
811 *and Physics*, 19, 8569-8590, 10.5194/acp-19-8569-2019, 2019.

812 Kong, L., Hu, M., Tan, Q., Feng, M., Qu, Y., An, J., Zhang, Y., Liu, X., Cheng, N., Deng,
813 Y., Zhai, R., and Wang, Z.: Key role of atmospheric water content in the
814 formation of regional haze in southern China, *Atmospheric Environment*, 216,
815 116918, 10.1016/j.atmosenv.2019.116918, 2019.

816 Kong, L., Hu, M., Tan, Q., Feng, M., Qu, Y., An, J., Zhang, Y., Liu, X., and Cheng, N.:
817 Aerosol optical properties under different pollution levels in the Pearl River
818 Delta (PRD) region of China, *Journal of Environmental Sciences*, 87, 49-59,
819 10.1016/j.jes.2019.02.019, 2020.

820 Li, K., Jacob, D. J., Liao, H., Zhu, J., Shah, V., Shen, L., Bates, K. H., Zhang, Q., and
821 Zhai, S.: A two-pollutant strategy for improving ozone and particulate air
822 quality in China, *Nature Geoscience*, 10.1038/s41561-019-0464-x, 2019a.

823 Li, L., Tan, Q., Zhang, Y., Feng, M., Qu, Y., An, J., and Liu, X.: Characteristics and
824 source apportionment of PM_{2.5} during persistent extreme haze events in
825 Chengdu, southwest China, *Environmental Pollution*, 230, 718-729,
826 10.1016/j.envpol.2017.07.029, 2017.

827 Li, M., Wang, T., Xie, M., Li, S., Zhuang, B., Huang, X., Chen, P., Zhao, M., and Liu,
828 J.: Formation and Evolution Mechanisms for Two Extreme Haze Episodes in

带格式的: 字体: (中文)+中文正文 (等线)

829 the Yangtze River Delta Region of China During Winter 2016, *Journal of*
830 *Geophysical Research: Atmospheres*, 124, 3607-3623, 10.1029/2019jd030535,
831 2019b.

832 Li, Y., Ye, C., Liu, J., Zhu, Y., Wang, J., Tan, Z., Lin, W., Zeng, L., and Zhu, T.:
833 Observation of regional air pollutant transport between the megacity Beijing
834 and the North China Plain, *Atmospheric Chemistry and Physics*, 16, 14265-
835 14283, 10.5194/acp-16-14265-2016, 2016.

836 Liu, K., Wu, Q., Wang, L., Wang, S., Liu, T., Ding, D., Tang, Y., Li, G., Tian, H., Duan,
837 L., Wang, X., Fu, X., Feng, X., and Hao, J.: Measure-Specific Effectiveness of
838 Air Pollution Control on China's Atmospheric Mercury Concentration and
839 Deposition during 2013-2017, *Environmental Science & Technology*, 53, 8938-
840 8946, 10.1021/acs.est.9b02428, 2019a.

841 Liu, L., Zhang, X., Wong, A. Y. H., Xu, W., Liu, X., Li, Y., Mi, H., Lu, X., Zhao, L.,
842 Wang, Z., Wu, X., and Wei, J.: Estimating global surface ammonia
843 concentrations inferred from satellite retrievals, *Atmospheric Chemistry and*
844 *Physics*, 19, 12051-12066, 10.5194/acp-19-12051-2019, 2019b.

845 Liu, M., Huang, X., Song, Y., Tang, J., Cao, J., Zhang, X., Zhang, Q., Wang, S., Xu, T.,
846 Kang, L., Cai, X., Zhang, H., Yang, F., Wang, H., Yu, J. Z., Lau, A. K. H., He,
847 L., Huang, X., Duan, L., Ding, A., Xue, L., Gao, J., Liu, B., and Zhu, T.:
848 Ammonia emission control in China would mitigate haze pollution and nitrogen
849 deposition, but worsen acid rain, *Proceedings of the National Academy of*
850 *Sciences of the United States of America*, 116, 7760-7765,
851 10.1073/pnas.1814880116, 2019c.

852 Liu, X., Zhang, Y., Cheng, Y., Hu, M., and Han, T.: Aerosol hygroscopicity and its
853 impact on atmospheric visibility and radiative forcing in Guangzhou during the
854 2006 PRIDE-PRD campaign, *Atmospheric Environment*, 60, 59-67,
855 10.1016/j.atmosenv.2012.06.016, 2012.

856 Liu, X., Li, J., Qu, Y., Han, T., Hou, L., Gu, J., Chen, C., Yang, Y., Yang, T., and Zhang,
857 Y.: Formation and evolution mechanism of regional haze: A case study in the
858 megacity Beijing, China, *Atmospheric Chemistry and Physics*, 13, 4501-4514,
859 [10.5194/acp-13-4501-2013](https://doi.org/10.5194/acp-13-4501-2013), 2013a.

860 Liu, X., Zhang, Y., Han, W., Tang, A., Shen, J., Cui, Z., Vitousek, P., Erisman, J. W.,
861 Goulding, K., Christie, P., Fangmeier, A., and Zhang, F.: Enhanced nitrogen
862 deposition over China, *Nature*, 494, 459-462, 10.1038/nature11917, 2013b.

863 Liu, Y., Zheng, M., Yu, M., Cai, X., Du, H., Li, J., Zhou, T., Yan, C., Wang, X., Shi, Z.,
864 Harrison, R. M., Zhang, Q., and He, K.: High-time-resolution source
865 apportionment of PM_{2.5} in Beijing with multiple models, *Atmospheric*
866 *Chemistry and Physics*, 19, 6595-6609, 10.5194/acp-19-6595-2019, 2019d.

867 Malm, W. C., and Hand, J. L.: An examination of the physical and optical properties of
868 aerosols collected in the IMPROVE program, *Atmospheric Environment*, 41,
869 3407-3427, 10.1016/j.atmosenv.2006.12.012, 2007.

870 Meier, J., Wehner, B., Massling, A., Birmili, W., Nowak, A., Gnauk, T., Brüeggemann,

871 E., Herrmann, H., Min, H., and Wiedensohler, A.: Hygroscopic growth of urban
872 aerosol particles in Beijing (China) during wintertime: a comparison of three
873 experimental methods, *Atmospheric Chemistry and Physics*, 9, 6865-6880,
874 10.5194/acp-9-6865-2009, 2009.

875 Ministry of Ecology and Environment of the People's Republic of China: Detailed
876 regulations for the implementation of air pollution control action plan in Beijing,
877 Tianjin, Hebei and surrounding areas, 2013. Website:
878 http://www.mee.gov.cn/gkml/hbb/bwj/201309/t20130918_260414.htm, last
879 access: June 17, 2020.

880 National Aeronautics and Space Administration: Giovanni data, 2019. Website :
881 <https://giovanni.gsfc.nasa.gov/giovanni/>, last access: June 17, 2020.

882 National Oceanic and Atmospheric Administration: HYSPLIT data, 2019. Website:
883 <ftp://arlftp.arlhq.noaa.gov/pub/archives/gdas1>, last access: June 17, 2020.

884 Ohta, S., and Okita, T.: A chemical characterization of atmospheric aerosol in Sapporo,
885 *Atmospheric Environment Part A General Topics*, 24, 815-822, [10.1016/0960-](https://doi.org/10.1016/0960-1686(90)90282-R)
886 [1686\(90\)90282-R](https://doi.org/10.1016/0960-1686(90)90282-R), 1990.

887 Pan, Y., Tian, S., Liu, D., Fang, Y., Zhu, X., Zhang, Q., Zheng, B., Michalski, G., and
888 Wang, Y.: Fossil Fuel Combustion-Related Emissions Dominate Atmospheric
889 Ammonia Sources during Severe Haze Episodes: Evidence from N-15-Stable
890 Isotope in Size-Resolved Aerosol Ammonium, *Environmental Science &*
891 *Technology*, 50, 8049-8056, 10.1021/acs.est.6b00634, 2016.

892 Peng, G., Wang, X., Wu, Z., Wang, Z., Yang, L., Zhong, L., and Chen, D.:
893 Characteristics of particulate matter pollution in the Pearl River Delta region,
894 China: an observational-based analysis of two monitoring sites, *Journal of*
895 *Environmental Monitoring*, 13, 1927-1934, 10.1039/c0em00776e, 2011.

896 Qiao, X., Guo, H., Tang, Y., Wang, P., Deng, W., Zhao, X., Hu, J., Ying, Q., and Zhang,
897 H.: Local and regional contributions to fine particulate matter in the 18 cities of
898 Sichuan Basin, southwestern China, *Atmospheric Chemistry and Physics*, 19,
899 5791-5803, 10.5194/acp-19-5791-2019, 2019.

900 Qin, W., Zhang, Y., Chen, J., Yu, Q., Cheng, S., Li, W., Liu, X., and Tian, H.: Variation,
901 sources and historical trend of black carbon in Beijing, China based on ground
902 observation and MERRA-2 reanalysis data, *Environmental Pollution*, 245, 853-
903 863, 10.1016/j.envpol.2018.11.063, 2019.

904 Song, M., Tan, Q., Feng, M., Qu, Y., Liu, X., An, J., and Zhang, Y.: Source
905 apportionment and secondary transformation of atmospheric non-methane
906 hydrocarbons in Chengdu, southwest China, *Journal of Geophysical Research:*
907 *Atmospheres*, 123, 9741-9763, [10.1029/2018JD028479](https://doi.org/10.1029/2018JD028479), 2018.

908 Sun, Y., Zhuang, G., Tang, A. A., Wang, Y., and An, Z.: Chemical characteristics of
909 PM_{2.5} and PM₁₀ in haze-fog episodes in Beijing, *Environmental Science &*
910 *Technology*, 40, 3148-3155, [10.1021/es051533g](https://doi.org/10.1021/es051533g), 2006.

911 Sun, Y., Wang, Z., Fu, P., Jiang, Q., Yang, T., Li, J., and Ge, X.: The impact of relative
912 humidity on aerosol composition and evolution processes during wintertime in

913 Beijing, China, Atmospheric Environment, 77, 927-934,
914 10.1016/j.atmosenv.2013.06.019, 2013.

915 Sun, Y., Jiang, Q., Wang, Z., Fu, P., Li, J., Yang, T., and Yin, Y.: Investigation of the
916 sources and evolution processes of severe haze pollution in Beijing in January
917 2013, Journal of Geophysical Research: Atmospheres, 119, 4380-4398,
918 10.1002/2014jd021641, 2014.

919 The People's Government of Sichuan Province: Detailed rules for the implementation
920 of the action plan for the prevention and control of air pollution in Sichuan
921 Province 2015 annual implementation plan, in, 2015. Website :
922 <http://www.sc.gov.cn/10462/10883/11066/2015/4/22/10333390.shtml> , last
923 access: June 17 2020.

924 The People's Government of Sichuan Province: Detailed rules for the implementation
925 of the action plan for the prevention and control of air pollution in Sichuan
926 Province 2016 annual implementation plan, in, 2016. Website :
927 [http://www.sc.gov.cn/zcwj/xxgk/NewT.aspx?i=20160401095908-612769-00-
928 000](http://www.sc.gov.cn/zcwj/xxgk/NewT.aspx?i=20160401095908-612769-00-000) , last access: June 17 2020.

929 The People's Government of Sichuan Province: Detailed rules for the implementation
930 of the action plan for the prevention and control of air pollution in Sichuan
931 Province 2017 annual implementation plan, in, 2017. Website :
932 [http://www.sc.gov.cn/zcwj/xxgk/NewT.aspx?i=20170527091543-450025-00-
933 000](http://www.sc.gov.cn/zcwj/xxgk/NewT.aspx?i=20170527091543-450025-00-000) , last access: June 17 2020.

934 the State Council: Three-Year Action Plan for Winning the Blue Sky Defense Battle,
935 2018. Website : [http://www.gov.cn/zhengce/content/2018-
936 07/03/content_5303158.htm](http://www.gov.cn/zhengce/content/2018-07/03/content_5303158.htm), last access: June 17 2020.

937 Tian, Y., Xiao, Z., Wang, H., Xing, P., Liao, G., Huangfu, Y., Shi, G., Chen, K., Bi, X.,
938 and Feng, Y.: Influence of the sampling period and time resolution on the PM
939 source apportionment: Study based on the high time-resolution data and long-
940 term daily data, Atmospheric Environment, 165, 301-309,
941 [10.1016/j.atmosenv.2017.07.003](https://doi.org/10.1016/j.atmosenv.2017.07.003), 2017.

942 Tie, X., Wu, D., and Brasseur, G.: Lung cancer mortality and exposure to atmospheric
943 aerosol particles in Guangzhou, China, Atmospheric Environment, 43, 2375-
944 2377, [10.1016/j.atmosenv.2009.01.036](https://doi.org/10.1016/j.atmosenv.2009.01.036), 2009.

945 Tie, X., Huang, R. J., Cao, J., Zhang, Q., Cheng, Y., Su, H., Chang, D., Poschl, U.,
946 Hoffmann, T., Dusek, U., Li, G., Worsnop, D. R., and O'Dowd, C. D.: Severe
947 Pollution in China Amplified by Atmospheric Moisture, Scientific Reports, 7,
948 15760, 10.1038/s41598-017-15909-1, 2017.

949 Tong, D., Geng, G., Jiang, K., Cheng, J., Zheng, Y., Hong, C., Yan, L., Zhang, Y., Chen,
950 X., Bo, Y., Lei, Y., Zhang, Q., and He, K.: Energy and emission pathways
951 towards PM2.5 air quality attainment in the Beijing-Tianjin-Hebei region by
952 2030, Science of the Total Environment, 692, 361-370,
953 10.1016/j.scitotenv.2019.07.218, 2019.

954 Uria-Tellaetxe, I., and Carslaw, D. C.: Conditional bivariate probability function for

955 source identification, *Environmental Modelling & Software*, 59, 1-9,
956 [10.1016/j.envsoft.2014.05.002](https://doi.org/10.1016/j.envsoft.2014.05.002), 2014.

957 Walker, J. T., Whittall, D. R., Robarge, W., and Paerl, H. W.: Ambient ammonia and
958 ammonium aerosol across a region of variable ammonia emission density,
959 *Atmospheric Environment*, 38, 1235-1246, [10.1016/j.atmosenv.2003.11.027](https://doi.org/10.1016/j.atmosenv.2003.11.027),
960 2004.

961 Wang, G., Zhang, R., Gomez, M. E., Yang, L., Levy, Z. M., Hu, M., Lin, Y., Peng, J.,
962 Guo, S., Meng, J., and Li, J.: Persistent sulfate formation from London Fog to
963 Chinese haze, *Proceedings of the National Academy of Sciences of the United
964 States of America*, 48, 13630-13635, [10.1073/pnas.1616540113](https://doi.org/10.1073/pnas.1616540113), 2016.

965 Wang, L., Li, W., Sun, Y., Tao, M., Xin, J., Song, T., Li, X., Zhang, N., Ying, K., and
966 Wang, Y.: PM_{2.5} Characteristics and Regional Transport Contribution in Five
967 Cities in Southern North China Plain, During 2013–2015, *Atmosphere*, 9, 157,
968 [10.3390/atmos9040157](https://doi.org/10.3390/atmos9040157), 2018.

969 Wang, Q., Zhuang, G., Kan, H., Liu, T., Deng, C., Jian, X., Lin, Y., Guo, Z., Ying, C.,
970 and Fu, Q.: Probing the severe haze pollution in three typical regions of China:
971 Characteristics, sources and regional impacts, *Atmospheric Environment*, 120,
972 76-88, [10.1016/j.atmosenv.2015.08.076](https://doi.org/10.1016/j.atmosenv.2015.08.076), 2015.

973 Wang, Y., Li, W., Gao, W., Liu, Z., Tian, S., Shen, R., Ji, D., Wang, S., Wang, L., Tang,
974 G., Song, T., Cheng, M., Wang, G., Gong, Z., Hao, J., and Zhang, Y.: Trends in
975 particulate matter and its chemical compositions in China from 2013-2017,
976 *Science China Earth Sciences*, 62, 1857-1871, [10.1007/s11430-018-9373-1](https://doi.org/10.1007/s11430-018-9373-1),
977 2019.

978 Wang, Y. Q., Zhang, X. Y., and Draxler, R. R.: TrajStat: GIS-based software that uses
979 various trajectory statistical analysis methods to identify potential sources from
980 long-term air pollution measurement data, *Environmental Modelling &
981 Software*, 24, 938-939, [10.1016/j.envsoft.2009.01.004](https://doi.org/10.1016/j.envsoft.2009.01.004), 2009.

982 Yang, Y., Liu, X., Qu, Y., An, J., Jiang, R., Zhang, Y. H., Sun, Y. L., Wu, Z. J., Zhang,
983 F., Xu, W. Q., and Ma, Q. X.: Characteristics and formation mechanism of
984 continuous hazes in China: a case study during the autumn of 2014 in the North
985 China Plain, *Atmospheric Chemistry and Physics*, 15, 8165-8178, [10.5194/acp-
986 15-8165-2015](https://doi.org/10.5194/acp-15-8165-2015), 2015a.

987 Yang, Y., Liu, X., Qu, Y., Wang, J., An, J., Zhang, Y., and Zhang, F.: Formation
988 mechanism of continuous extreme haze episodes in the megacity Beijing, China,
989 in January 2013, *Atmospheric Research*, 155, 192-203,
990 [10.1016/j.atmosres.2014.11.023](https://doi.org/10.1016/j.atmosres.2014.11.023), 2015b.

991 Yao, L., Garmash, O., Bianchi, F., Zheng, J., Yan, C., Kontkanen, J., Junninen, H.,
992 Mazon, S. B., Ehn, M., Paasonen, P., Sipila, M., Wang, M., Wang, X., Xiao, S.,
993 Chen, H., Lu, Y., Zhang, B., Wang, D., Fu, Q., Geng, F., Li, L., Wang, H., Qiao,
994 L., Yang, X., Chen, J., Kerminen, V.-M., Petaja, T., Worsnop, D. R., Kulmala,
995 M., and Wang, L.: Atmospheric new particle formation from sulfuric acid and
996 amines in a Chinese megacity, *Science*, 361, 278-281, [10.1126/science.aao4839](https://doi.org/10.1126/science.aao4839),

997 2018.

998 Zhang, H., Cheng, S., Li, J., Yao, S., and Wang, X.: Investigating the aerosol mass and
999 chemical components characteristics and feedback effects on the meteorological
1000 factors in the Beijing-Tianjin-Hebei region, China, *Environmental Pollution*,
1001 244, 495-502, 10.1016/j.envpol.2018.10.087, 2019a.

1002 Zhang, L., Guo, X., Zhao, T., Gong, S., Xu, X., Li, Y., Luo, L., Gui, K., Wang, H.,
1003 Zheng, Y., and Yin, X.: A modelling study of the terrain effects on haze pollution
1004 in the Sichuan Basin, *Atmospheric Environment*, 196, 77-85,
1005 10.1016/j.atmosenv.2018.10.007, 2019b.

1006 Zhang, R., Wang, G., Guo, S., Zamora, M. L., Ying, Q., Lin, Y., Wang, W., Hu, M., and
1007 Wang, Y.: Formation of urban fine particulate matter, *Chemical Reviews*, 115,
1008 3803-3855, [10.1021/acs.chemrev.5b00006](https://doi.org/10.1021/acs.chemrev.5b00006), 2015.

1009 Zhang, Y., Chen, J., Yang, H., Li, R., and Yu, Q.: Seasonal variation and potential source
1010 regions of PM_{2.5}-bound PAHs in the megacity Beijing, China: Impact of
1011 regional transport, *Environmental Pollution*, 231, 329-338,
1012 10.1016/j.envpol.2017.08.025, 2017.

1013 Zhang, Y., Xue, M., Zhu, K., and Zhou, B.: What Is the Main Cause of Diurnal Variation
1014 and Nocturnal Peak of Summer Precipitation in Sichuan Basin, China? The Key
1015 Role of Boundary Layer Low-Level Jet Inertial Oscillations, *Journal of
1016 Geophysical Research: Atmospheres*, 124, 2643-2664, 10.1029/2018jd029834,
1017 2019c.

1018 Zhao, B., Zheng, H., Wang, S., Smith, K. R., Lu, X., Aunan, K., Gu, Y., Wang, Y., Ding,
1019 D., Xing, J., Fu, X., Yang, X., Liou, K.-N., and Hao, J.: Change in household
1020 fuels dominates the decrease in PM_{2.5} exposure and premature mortality in
1021 China in 2005-2015, *Proceedings of the National Academy of Sciences of the
1022 United States of America*, 115, 12401-12406, 10.1073/pnas.1812955115, 2018.

1023 Zhao, H., Li, X., Zhang, Q., Jiang, X., Lin, J., Peters, G. G., Li, M., Geng, G., Zheng,
1024 B., Huo, H., Zhang, L., Wang, H., Davis, S. J., and He, K.: Effects of
1025 atmospheric transport and trade on air pollution mortality in China,
1026 *Atmospheric Chemistry and Physics*, 17, 10367-10381, 10.5194/acp-17-10367-
1027 2017, 2017.

1028 Zheng, G., Duan, F., Ma, Y., Zhang, Q., Huang, T., Kimoto, T., Cheng, Y., Su, H., and
1029 He, K.: Episode-Based Evolution Pattern Analysis of Haze Pollution: Method
1030 Development and Results from Beijing, China, *Environmental Science &
1031 Technology*, 50, 4632-4641, 10.1021/acs.est.5b05593, 2016.

1032 Zheng, H., Kong, S. F., Yan, Q., Wu, F. Q., Cheng, Y., Zheng, S. R., Wu, J., Yang, G.
1033 W., Zheng, M. M., Tang, L. L., Yin, Y., Chen, K., Zhao, T. L., Liu, D. T., Li, S.
1034 L., Qi, S. H., Zhao, D. L., Zhang, T., Ruan, J. J., and Huang, M. Z.: The impacts
1035 of pollution control measures on PM_{2.5} reduction: Insights of chemical
1036 composition, source variation and health risk, *Atmospheric Environment*, 197,
1037 103-117, 10.1016/j.atmosenv.2018.10.023, 2019.

1038 Zhong, J., Zhang, X., Wang, Y., Wang, J., Shen, X., Zhang, H., Wang, T., Xie, Z., Liu,

1039 C., Zhang, H., Zhao, T., Sun, J., Fan, S., Gao, Z., Li, Y., and Wang, L.: The two-
1040 way feedback mechanism between unfavorable meteorological conditions and
1041 cumulative aerosol pollution in various haze regions of China, *Atmospheric*
1042 *Chemistry and Physics*, 19, 3287-3306, 10.5194/acp-19-3287-2019, 2019.
1043 Zhu, J., Chen, L., Liao, H., and Dang, R.: Correlations between PM_{2.5} and Ozone over
1044 China and Associated Underlying Reasons, *Atmosphere*, 10, 352,
1045 10.3390/atmos10070352, 2019.